Chemical Geology 622 (2023) 121355

Contents lists available at ScienceDirect

Chemical Geology

journal homepage: www.elsevier.com/locate/chemgeo

# Ba/Ca of stylasterid coral skeletons records dissolved seawater barium concentrations

James Kershaw [a,*], Joseph A. Stewart [a,b], Ivo Strawson [a,c], Maria Luiza de Carvalho Ferreira [a,d], Laura F. Robinson [a], Katharine R. Hendry [a,e], Ana Samperiz [a,f], Andrea Burke [g], James W.B. Rae [g], Rusty D. Day [b,h], Peter J. Etnoyer [i], Branwen Williams [j], Vreni Häussermann [k]

[a] School of Earth Sciences, University of Bristol, Queens Road, Bristol BS8 1RJ, UK
[b] National Institute of Standards and Technology, Chemical Science Division, Hollings Marine Laboratory, Charleston, SC, USA
[c] Department of Earth Sciences, University of Cambridge, Downing Street, Cambridge CB2 3EQ, UK
[d] Department of the Geophysical Sciences, University of Chicago, 5734 S. Ellis Avenue, Chicago, IL 60637, USA
[e] British Antarctic Survey, Cambridge CB3 0ET, UK
[f] School of Earth and Environmental Sciences, Cardiff University, Cardiff CF10 3AT, UK
[g] School of Earth & Environmental Science, University of St Andrews, Bute Building, St Andrews KY16 9TS, UK
[h] Marine Science and Nautical Training Academy (MANTA), 417 Planters Trace Dr, Charleston, SC 29412, USA
[i] NOAA National Centers for Coastal Ocean Science, Charleston, SC 29412, USA
[j] Keck Science Department, Claremont McKenna-Pitzer-Scripps Colleges, Claremont, CA 91711, USA
[k] Pontificia Universidad Católica de Valparaíso, Escuela de Ciencias del Mar, Facultad de Recursos Naturales, Valparaíso, Chile

ARTICLE INFO

Editor: Michael E. Boettcher

*Keywords:*
Ba/Ca
Barium
Scleractinia
Stylasteridae
Coral

ABSTRACT

The concentration of dissolved barium in seawater ($[Ba]_{SW}$) is influenced by both primary productivity and ocean circulation patterns. Reconstructing past subsurface $[Ba]_{SW}$ can therefore provide important information on processes which regulate global climate. Previous Ba/Ca measurements of scleractinian and bamboo deep-sea coral skeletons exhibit linear relationships with $[Ba]_{SW}$, acting as archives for past Ba cycling. However, skeletal Ba/Ca ratios of the Stylasteridae – a group of widely distributed, azooxanthellate, hydrozoan coral – have not been previously studied.

Here, we present Ba/Ca ratios of modern stylasterid (aragonitic, calcitic and mixed mineralogy) and azooxanthellate scleractinian skeletons, paired with published proximal hydrographic data. We find that $[Ba]_{SW}$ and sample mineralogy are the primary controls on stylasterid Ba/Ca, while seawater temperature exerts a weak secondary control. $[Ba]_{SW}$ also exerts a strong control on azooxanthellate scleractinian Ba/Ca. However, Ba-incorporation into scleractinian skeletons varies between locations and across depth gradients, and we find a more sensitive relationship between scleractinian Ba/Ca and $[Ba]_{SW}$ than previously reported.

Paired Sr/Ca measurements suggest that this variability in scleractinian Ba/Ca may result from the influence of varying degrees of Rayleigh fractionation during calcification. We find that these processes exert a smaller influence on Ba-incorporation into stylasterid coral skeletons, a result consistent with other aspects of their skeletal geochemistry. Stylasterid Ba/Ca ratios are therefore a powerful, novel archive of past changes in $[Ba]_{SW}$, particularly when measured in combination with temperature sensitive tracers such as Li/Mg or Sr/Ca. Indeed, with robust $[Ba]_{SW}$ and temperature proxies now established, stylasterids have the potential to be an important new archive for palaeoceanographic studies.

## 1. Introduction

The dissolved concentration of barium in seawater ($[Ba]_{SW}$) has a nutrient-like profile with depth (Chan et al., 1977; Jeandel et al., 1996). Scavenging by sinking particles and the formation of barite associated with aggregated organic matter largely removes dissolved Ba from the shallow ocean, while the subsequent regeneration of barite below its saturation horizon results in increasing $[Ba]_{SW}$ with depth (e.g. Dehairs

* Corresponding author.
*E-mail address:* james.kershaw@bristol.ac.uk (J. Kershaw).

https://doi.org/10.1016/j.chemgeo.2023.121355
Received 24 August 2022; Received in revised form 3 January 2023; Accepted 29 January 2023
Available online 1 February 2023

et al., 1980; Collier and Edmond, 1984; Bishop, 1988; Dymond et al., 1992; Ganeshram et al., 2003; Sternberg et al., 2005; Tang and Morel, 2006; Griffith and Paytan, 2012). The coupling between the cycling of barite and organic matter results in a link between $[Ba]_{SW}$ at shallow depths and regional primary productivity (Horner et al., 2015; Bates et al., 2017). Additionally, surface ocean $[Ba]_{SW}$ is sensitive to the position of oceanic fronts, perhaps in response to differing phytoplankton assemblages (Pyle et al., 2018). In high-latitude regions, shallow waters sink to form the major deep-water masses which fill the interior ocean basins. Below the depths of barite formation, $[Ba]_{SW}$ is primarily controlled by conservative mixing of these deep-water masses, combined with non-conservative addition and/or removal of Ba along the water-mass flow path (Horner et al., 2015; Bates et al., 2017). Reconstructing past changes in subsurface $[Ba]_{SW}$ therefore has the potential to constrain past variations in these important oceanographic processes.

The skeletal Ba/Ca ratio of marine biogenic carbonates including foraminifera, bivalves and both shallow- and deep-water corals has been shown to covary with $[Ba]_{SW}$, facilitating the use of these ratios in palaeoceanography (e.g. Lea et al., 1989; Lea and Spero, 1994; Anagnostou et al., 2011; Hönisch et al., 2011; LaVigne et al., 2011; Poulain et al., 2015; LaVigne et al., 2016; Spooner et al., 2018). In subsurface environments, Ba/Ca ratios of azooxanthellate coral groups are of particular interest, with linear relationships established between $[Ba]_{SW}$ and skeletal Ba/Ca of azooxanthellate scleractinian (Anagnostou et al., 2011; Spooner et al., 2018) and bamboo corals (LaVigne et al., 2011; Thresher et al., 2016).

However, there remain unexplained aspects of Ba-incorporation into azooxanthellate corals. For instance, azooxanthellate scleractinian Ba partition coefficients ($D_{Ba}$ = Ba/$Ca_{coral}$ / Ba/$Ca_{seawater}$) vary systematically with $[Ba]_{SW}$ (Spooner et al. 2018), while scleractinian corals collected from the Rekyjanes Ridge (south of Iceland) have lower $D_{Ba}$ values than those from other locations (Hemsing et al., 2018; Spooner et al., 2018). Additionally, bamboo corals display a negative relationship between coral $D_{Ba}$ and water depth (Geyman et al., 2019). This suggests that Ba-incorporation into azooxanthellate coral skeletons may be influenced by biological mediation of the coral calcification process (Spooner et al., 2018; Geyman et al., 2019).

Scleractinian corals calcify from a partially-enclosed calcification fluid, whose carbonate chemistry is modified by Ca-ATPase pumping to promote mineralisation (Al-Horani et al., 2003; Sinclair and Risk, 2006). The balance between coral growth rate, replenishment of the calcifying fluid with external seawater, and ion pumping, can alter the composition of the coral skeleton by Rayleigh fractionation processes (e.g. Gaetani and Cohen, 2006; Gagnon et al., 2007), which may explain variations in Ba/Ca ratios in zooxanthellate scleractinian (Gaetani and Cohen, 2006; Reed et al., 2021) and azooxanthellate bamboo corals (Geyman et al. 2019). Additionally, coprecipitation of witherite ($BaCO_3$) within the domains of aragonite may also occur due to high degrees of carbonate oversaturation in the scleractinian calcifying fluid, leading to elevated Ba-incorporation into coral aragonite (Mavromatis et al., 2018; Liu et al., 2019). These biocalcification-related effects on coral Ba/Ca ratios have the potential to introduce uncertainty into reconstructions of past $[Ba]_{SW}$, and therefore require characterisation. Discussion of these themes has thus far been limited to anthozoan coral groups (including Scleractinia and bamboo corals), while Ba/Ca ratios of hydrozoan corals remain entirely unexplored.

Stylasteridae (Class Hydrozoa: Order Anthoathecata) are the second most diverse group of hard corals and are found across a wide bathymetric and geographic range (Cairns, 2007; Cairns, 2011). The vast majority of stylasterid species form calcium carbonate skeletons, constituting an important, substrate-forming component of shallow and deep marine ecosystems (Cairns 2011). Despite their widespread abundance and ecological importance, studies of stylasterids remain few, and their skeletal geochemistry is largely unknown.

Stylasterids can build their skeletons from aragonite, high-Mg calcite or a mixture of both polymorphs, with this suite of mineralogical variability found within individual stylasterid genera (Cairns and Macintyre, 1992; Samperiz et al., 2020). Stylasterid geochemistry can therefore be compared to both azooxanthellate scleractinian (aragonitic) and bamboo (high-Mg calcitic) corals, while controlling for their differing mineralogies. This also permits phylogenetically-controlled investigation of the role of mineralogy in determining coral geochemistry.

Recent studies reveal important distinctions between the geochemical composition of stylasterid and scleractinian skeletons. Stylasterid skeletal $\delta^{18}O$ and $\delta^{13}C$ are closer to equilibrium with seawater (Samperiz et al. 2020), while $\delta^{11}B$, U/Ca and B/Ca measurements suggest that stylasterids calcify from a fluid with pH and $[CO_3]^{2-}$ closer to seawater than Scleractinia (Stewart et al., 2022). Furthermore, stylasterid Li/Mg and Sr/Ca correlate more strongly with seawater temperature and appear less impacted by biological mediation of the calcification process (Stewart et al., 2020a). This combined evidence for reduced modification of the stylasterid calcifying fluid suggests that stylasterid skeletons may be particularly useful palaeoceanographic archives. In the case of Ba, other aspects of stylasterid skeletal geochemistry also suggest that the biologically mediated vital-effects impacting Ba-incorporation into scleractinian (Spooner et al., 2018) and bamboo (Geyman et al., 2019) corals, may be less pronounced in stylasterids.

Here we present the first measurements of stylasterid skeletal Ba/Ca, supplemented by new measurements of Ba/Ca from azooxanthellate Scleractinia. All Ba/Ca data are presented with paired Sr/Ca values (this study; Stewart et al., 2020a). Through inclusion of aragonitic, high-Mg calcitic and mixed mineralogy stylasterids, our data facilitate investigation of the biogenic and abiotic controls on Ba-incorporation into azooxanthellate stylasterid and scleractinian coral skeletons. By pairing Ba/Ca measurements with proximal $[Ba]_{SW}$ data (Fig. 1) we assess both

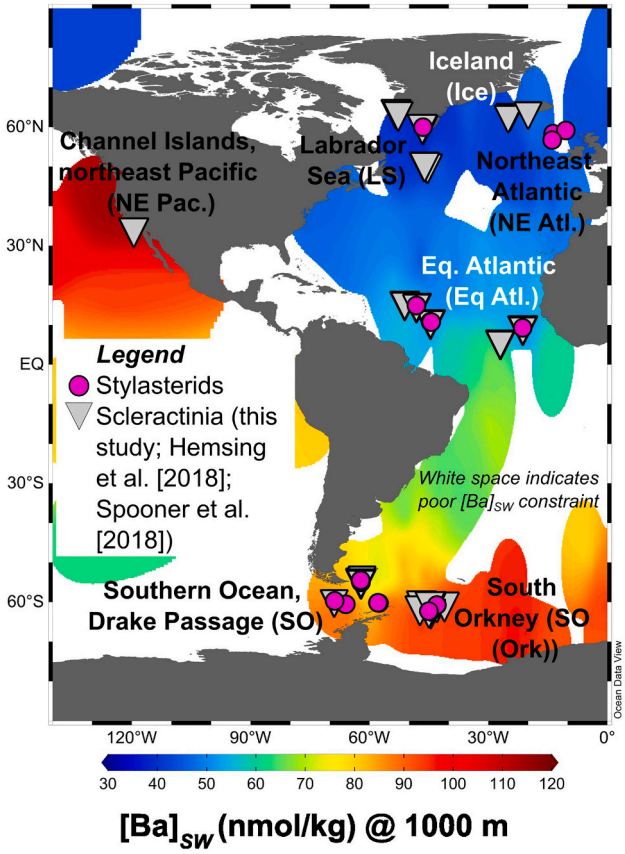


**Fig. 1.** Map showing coral locations overlain on $[Ba]_{SW}$ at 1000 m water depth. All stylasterids were measured in this study, Scleractinia include samples measured here and by previous work (Hemsing et al. 2018; Spooner et al. 2018). Location codes used throughout are shown in brackets. $[Ba]_{SW}$ data taken from sources listed in section 2.2, in addition to Falkner et al. [1994], Smetacek et al. [1997] and Hsieh and Henderson [2017]. Figure made using Ocean Data View software (Schlitzer, 2022).

the biomineralisation mechanisms and palaeoceanographic utility of these different coral groups.

## 2. Methods

### 2.1. Coral samples

We present new data from stylasterid ($n = 41$) and scleractinian ($n = 88$) coral skeletons. All corals were either collected alive (with associated organic tissue) or were preserved in "pristine" condition (i.e. no visible mineral or biological overgrowths or borings). Samples were collected from the Labrador Sea (LS; RRS *Discovery* DY081), the northeast Atlantic (NE Atl.; RRS *James Cook* JC136; R/V *Celtic Explorer* CE14001), the equatorial Atlantic (Eq. Atl.; RRS *James Cook* JC094), the Californian Channel Islands in the northeast Pacific (NE Pac.; NOAA ship *Bell M. Shimada* SH-15-03), the Drake Passage region of the Southern Ocean (SO; R/V *Nathaniel B. Palmer* 1103 and 0805; R/V *Laurence M. Gould* 0802) and the South Orkney Islands (SO (Ork); RRS *James Clark Ross* JR15005) (see Fig. 1).

We organise our sample set by both taxonomic affiliation and skeletal mineralogy (see section 2.3), and stylasterid samples include aragonitic (*Adelopora*, *Conopora, Errina, Errinopsis, Inferiolabiata* and *Stylaster*), high-Mg calcitic (*Cheiloporidion, Errina* and *Errinopsis*) and mixed mineralogy (*Errina*) corals. Nine scleractinian genera are included in this study (*Balanophyllia*, *Caryophyllia, Desmophyllum*, *Enallopsammia*, *Flabellum*, *Lophelia, Paraconotrochus, Solenosmilia and Vaughanella*). Our new scleractinian data were combined with previous work to create a compiled scleractinian dataset, spanning a range of locations (Fig. 1; Hemsing et al., 2018; Spooner et al., 2018). All relevant data (including sample metadata, paired hydrographic data and analytical data) are included in the Supplementary Information.

### 2.2. Hydrographic data

Proximal $[Ba]_{SW}$ data were compiled from published sources (GEOSECS data (corals paired with stations discussed or presented in Chan et al. [1977] and Östlund et al. [1987]); Hoppema et al., 2010; Roeske and Rutgers van der Loeff, 2012; Bates et al., 2017; Serrato Marks et al., 2017; Hemsing et al., 2018; Le Roy et al., 2018; Pyle et al., 2018; Geyman et al., 2019; GEOTRACES Intermediate Data Product Group, 2021). Where necessary, data reported in units of nM were converted to nmol/kg by assuming a seawater density of 1.025 kg/m$^3$ (i.e. assuming measurements were made at atmospheric pressure and ambient room temperature). For each coral sample, the geographically closest $[Ba]_{SW}$ profile was identified, before a representative $[Ba]_{SW}$ value was calculated by linearly interpolating between the nearest two measurement depths. $[Ba]_{SW}$ measurements in the modern ocean remain sparse, and some coral samples are more proximal to $[Ba]_{SW}$ measurements than others. The average distance between coral locations and the nearest $[Ba]_{SW}$ profile was less than 350 km (all distances reported in Supplementary Information). Uncertainty on matched $[Ba]_{SW}$ values was estimated using the largest of either the variability in values from the three most proximal measurements to each coral location (± 2 SD), or an analytical uncertainty of ±3 nmol/kg (calculated by applying a representative, high-end analytical uncertainty from the $[Ba]_{SW}$ datasets used (± 3%; e.g. Hemsing et al. [2018]) to the highest $[Ba]_{SW}$ value in our dataset (100 nmol/kg)). $[Ba]_{SW}$ values were converted to seawater Ba/Ca ratios (μmol/mol) using a seawater [Ca] value of 10.3 mmol/kg (Nozaki, 1997). Seawater [Ca] was assigned an error of ±5% to account for variations in salinity.

Coral samples were also paired with ancillary hydrographic data (temperature, salinity, concentrations of phosphate, dissolved silica and oxygen, alkalinity and dissolved inorganic carbon (DIC)). Data were taken from co-located CTD or ROV measurements where possible, or extracted from the GLODAP bottle database (Lauvset et al., 2021). Temperature uncertainties were estimated from the variability between the three most proximal measurements. Seawater pH (total scale) and aragonite saturation state ($\Omega_{arag.} = [Ca^{2+}]_{SW} \times [CO_3^{2-}]_{SW}/K^*_{sp}$) were calculated using the SEACARB package in R (Gattuso et al., 2021; input parameters were alkalinity and DIC, dissociation constants of carbonate taken from Lueker et al., 2000).

### 2.3. Specimen mineralogy

The skeletal mineralogy of four stylasterid samples (*Errina* sp. *(species: Errina gracilis)*, $n = 2$; *Errinopsis* sp. *(species: Errinopsis reticulum)*, n = 2) was measured using x-ray diffraction techniques (e.g. Kontoyannis and Vagenas, 2000; Dickinson and McGrath, 2001). Samples of 0.2 to 0.5 mg were cut using a diamond-coated rotary blade and ground to a fine powder using a pestle and mortar. X-ray diffraction measurements were made using a Bruker D8Advance diffractometer at the University of Manchester and the University of Bristol. Instrument settings used at the University of Manchester were wavelength (λ) = 1.54060 Å and 2θ ranging from 5 to 70, while at the University of Bristol, λ = 1.54056 Å and 2θ ranged from 10 to 55. The two samples of *Errina gracilis* are composed dominantly of aragonite, with minor calcite (5.5 to 7.0%). One sample of *Errinopsis reticulum* is composed entirely of aragonite, while the other is formed dominantly from calcite with minor (1%) aragonite.

The mineralogy of other stylasterid samples has either been directly measured previously ($n = 17$; Samperiz et al., 2020) or was inferred based on published data for that species ($n = 20$; Cairns and Macintyre, 1992; Samperiz et al., 2020). High-Mg calcitic stylasterid corals have Sr/Ca ratios ~4 times lower than aragonitic specimens (Stewart et al., 2020a), and these ratios were also used to check specimen mineralogy. All scleractinian samples were assumed to be aragonitic besides one sample from the genus *Paraconotrocus*, which contains both aragonite and high-Mg calcite (Stolarski et al., 2021).

### 2.4. Element/Ca measurements: sample preparation

Coral samples were air dried and organic matter removed by physical scraping and treatment in dilute $NaClO_4$. A diamond-coated rotary blade was used to cut pieces of each coral for analysis. Large (e.g. 0.1 to 1 g; ~ 0.5 cm × 0.5 cm) pieces of coral were sampled to reduce the effect of intra-skeletal variability (e.g. Gagnon et al., 2007). The apical tips of stylasterid branches were also avoided, since these may be further from equilibrium with seawater than the rest of the stylasterid skeleton (Samperiz et al. 2020). Photos showing examples of sampling are included in the Supplementary Information. Samples were ground to a fine powder using a pestle and mortar, and ~ 5 mg aliquots of each powder taken for analysis. Two replicate samples were taken for each coral, with each replicate cut, cleaned, dissolved and analysed separately. Additional samples of two mixed mineralogy *Errina* sp. corals were taken for cleaning experiments.

All samples were cleaned using a warm 1% $H_2O_2$ (80 °C; buffered in $NH_4OH$) oxidative leach to remove organic matter (adapted from Boyle, 1981; Barker et al., 2003; Rae et al., 2011). At this stage, three samples of mixed mineralogy stylasterids from the genus *Errina* (JR15005–113-2421-Egr2421 (1 set of replicates) and JR15005–113-2426-Egr2426 (2 sets of replicates)) were dried, and half of each transferred to a new acid cleaned vial for additional cleaning. These new aliquots were treated with a warm, 0.002 M diethylene-triaminepentaacetic acid (DTPA) solution buffered to approximately neutral pH by 0.2 M NaOH (Lea and Boyle, 1991; Lea and Boyle, 1993; Bates, 2016). DTPA is a chelating agent, capable of dissolving contaminant barite (barium sulphate) by complexing Ba. After treatment, these samples were thoroughly rinsed using concentrated ammonia solution followed by Milli-Q (Lea and Boyle, 1993). All samples (both oxidatively cleaned and those with additional DTPA treatment) were then transferred to new acid-leached vials and subjected to a weak acid leach (0.0005 M $HNO_3$) before dissolution in distilled 0.5 M $HNO_3$.

### 2.5. Element/Ca measurements: analytical techniques

Element/Ca analyses were carried out using similar techniques at the University of Bristol and the National Institute of Standards and Technology (NIST; Hollings Marine Lab) using a Thermo Element ICP-MS, or at the University of St Andrews using an Agilent 7500 ICP-MS. Intensities of $^{138}$Ba, $^{86}$Sr and $^{43}$Ca were measured in coral samples, blanks and well-characterised, synthetic calibrating standards to derive Ba/Ca and Sr/Ca ratios for coral samples.

Analytical reproducibility (RSD; 2 *s*) and accuracy were assessed using repeat measurements of NIST RM 8301 (Coral) (Stewart et al., 2020b) and (uncleaned) coral reference material JCp-1 (Hathorne et al., 2013). Long-term reproducibility on both materials was better than 2% (RSD; 2 *s*) for Ba/Ca and Sr/Ca. Small systematic analytical offsets (< 5%) between the labs and different calibrating standards used were quantified and corrected using NIST RM 8301 (Coral) results. To bring values into line with interlaboratory consensus values (Stewart et al., 2020b), Ba/Ca ratios measured at Bristol (BME bracketing standard), St Andrews, and at both NIST and Bristol (NBF bracketing standard) were adjusted by factors of 0.97, 1.03 and 0.95 respectively. Sr/Ca measurements from most samples used here have been published previously (using the same dissolved solutions, Stewart et al., 2020a). To facilitate comparison, all new Sr/Ca data were normalised to NIST RM 8301 (Coral) (Stewart et al., 2020b), using a small correction factor of 0.98. Reference material mean values, reproducibility and correction factors are summarised in the Supplementary Information.

Fe/Ca and Mn/Ca ratios were also measured to screen for the influence of non-carbonate phases including iron oxyhydroxides (e.g. Boyle, 1981). The effects of such phases on our coral Ba/Ca data are detailed in the Supplementary Information. In short, sample replicates with Fe/Ca ratios >40 mmol/mol were excluded, following the protocol in Spooner et al. [2018]. This resulted in 12 measurements from eight corals being removed from our dataset, which in practise had no effect on the principal findings of this study.

Our scleractinian Ba/Ca vs $[Ba]_{SW}$ relationship includes data from two previous studies (Spooner et al., 2018; Hemsing et al., 2018). These data were previously compiled with interlaboratory offsets accounted for using coral reference material JCp-1 (Spooner et al., 2018; see Supplementary Information for details). We find no clear analytical offsets between these previously published data (adjusted to JCp-1) and our own, justifying direct comparison of these datasets (Supplementary Information). Seven scleractinian samples measured in our study were replicates (different cut pieces) of corals analysed previously by Spooner et al. [2018] and/or Hemsing et al. [2018]. Results from each study were averaged.

### 2.6. Statistical analyses

For all relationships and regressions in this study, we use the Pearson correlation coefficient ($r$) to assess the degree of linear relationship between the two variables. $p$-values <0.05 were considered significant. We report the results of both Type I (Ordinary Least Squares; OLS) and Type II (Deming) regression analyses for both our Ba/Ca vs $[Ba]_{SW}$ and Sr/Ca vs temperature calibrations. OLS regression minimises the sum of the squared residuals in the y-variable (Ba/Ca or Sr/Ca) and assumes no uncertainty on the x variable ($[Ba]_{SW}$ or temperature). Conversely, unweighted Deming regression (equivalent to orthogonal regression) minimises the sum of the squared residuals orthogonal to the line of best fit, recognising that both the x and y regression variables have uncertainty. Deming regressions were performed using the deming package in R (Therneau, 2018), and assumed equal errors for all x and y variables.

## 3. Results

### 3.1. Coral Ba/Ca

Ba/Ca values of aragonitic stylasterid skeletons range from 7 to 19 μmol/mol, and samples span $[Ba]_{SW}$ from 40 to 100 nmol/kg. Ba partition coefficients ($D_{Ba}$) for stylasterid aragonite range from 1.5 to 2.3, with a mean value of 1.9 (± 0.4, 2SD). Calcitic stylasterid Ba/Ca is lower for a given $[Ba]_{SW}$, ranging from 8 to 15 μmol/mol and covering $[Ba]_{SW}$ from 60 to 100 nmol/kg. $D_{Ba}$ values for stylasterid calcite range from 1.3 to 1.6, with a lower mean value of 1.4 (± 0.2, 2SD).

Scleractinian Ba/Ca data presented here were combined with existing data from Spooner et al. [2018] and Hemsing et al. [2018] to create a full scleractinian dataset consisting of 156 individual corals, 78 of which were measured for the first time in this study. Ba/Ca values of the compiled dataset range from 7 to 24 μmol/mol, spanning $[Ba]_{SW}$ from 40 to 100 nmol/kg. Aragonitic scleractinian $D_{Ba}$ values range from 1.4 to 3.0, with a mean value of 2.0 (± 0.6, 2SD).

Four mixed mineralogy stylasterids have Ba/Ca values which are around 1 μmol/mol higher than entirely aragonitic stylasterids living in similar $[Ba]_{SW}$ conditions (Fig. 2a), corresponding to $D_{Ba}$ values of 2.2 to 2.3 (Fig. 3a). The mixed mineralogy scleractinian coral *Paraconotrochus* has a similar $D_{Ba}$ value of 2.3. Three additional replicate pairs of mixed mineralogy stylasterids were selected for further analysis to test for the presence of barium sulphate contaminant phases, as outlined in section 2.4. The choice of cleaning procedure had no effect on Ba/Ca ratios in these samples (Supplementary Information).

### 3.2. Coral Ba/Ca vs $[Ba]_{SW}$ calibrations

Stylasterid (aragonitic and high-Mg calcitic) and scleractinian (aragonite only) Ba/Ca ratios are linearly related to $[Ba]_{SW}$ (Fig. 2) by the regression relationships shown in Table 1. Mixed mineralogy corals were not used in regression analyses. For all taxa, OLS and Deming regressions produced gradients and intercepts within error of one another (Table 1). For the sake of simplicity and comparability with previous studies, we recommend using OLS regression calibrations for palaeoceanographic purposes. In practise, the choice of regression method makes no difference to our interpretations. Aragonitic stylasterids are more sensitive to changes in $[Ba]_{SW}$ than high-Mg calcitic stylasterids. For Scleractinia, our new relationship between Ba/Ca and $[Ba]_{SW}$ is significantly steeper than that reported previously by Spooner et al. [2018] (Table 1). $[Ba]_{SW}$ prediction intervals (95%) were narrowest for aragonitic stylasterids, and imply $[Ba]_{SW}$ can be reconstructed to better than 16 nmol/kg for all three coral taxa (Table 1).

### 3.3. Coral Sr/Ca

Sr/Ca data for most samples in this study have previously been published (Stewart et al., 2020a), and are in good agreement with the new stylasterid (n = 20) and scleractinian (n = 17) measurements. Aragonitic corals have higher Sr/Ca (average 10.8 mmol/mol) than corals formed from high-Mg calcite (average 3.0 mmol/mol). Previously reported relationships between seawater temperature and coral Sr/Ca (Stewart et al., 2020a) are within error of those including our new samples (Supplementary Information), and aragonitic stylasterid Sr/Ca retains a stronger correlation with temperature ($r = -0.80$) than Scleractinia ($r = -0.59$) (Supplementary Information). Subsample Sr/Ca and Ba/Ca ratios of mixed mineralogy corals are positively correlated in three out of four cases (Supplementary Information).

## 4. Discussion

### 4.1. $[Ba]_{SW}$ and sample mineralogy controls on stylasterid Ba/Ca

When split by mineralogy, stylasterid Ba/Ca ratios correlate strongly with $[Ba]_{SW}$ (Fig. 2a), suggesting that $[Ba]_{SW}$ exerts a dominant control on stylasterid Ba/Ca ratios. This result is not unexpected, given stylasterids calcify from a fluid derived directly from seawater (Stewart et al., 2022). As reflected in stylasterid $D_{Ba}$ values (Fig. 3a), high-Mg calcitic stylasterids contain less Ba than their aragonitic counterparts, and their

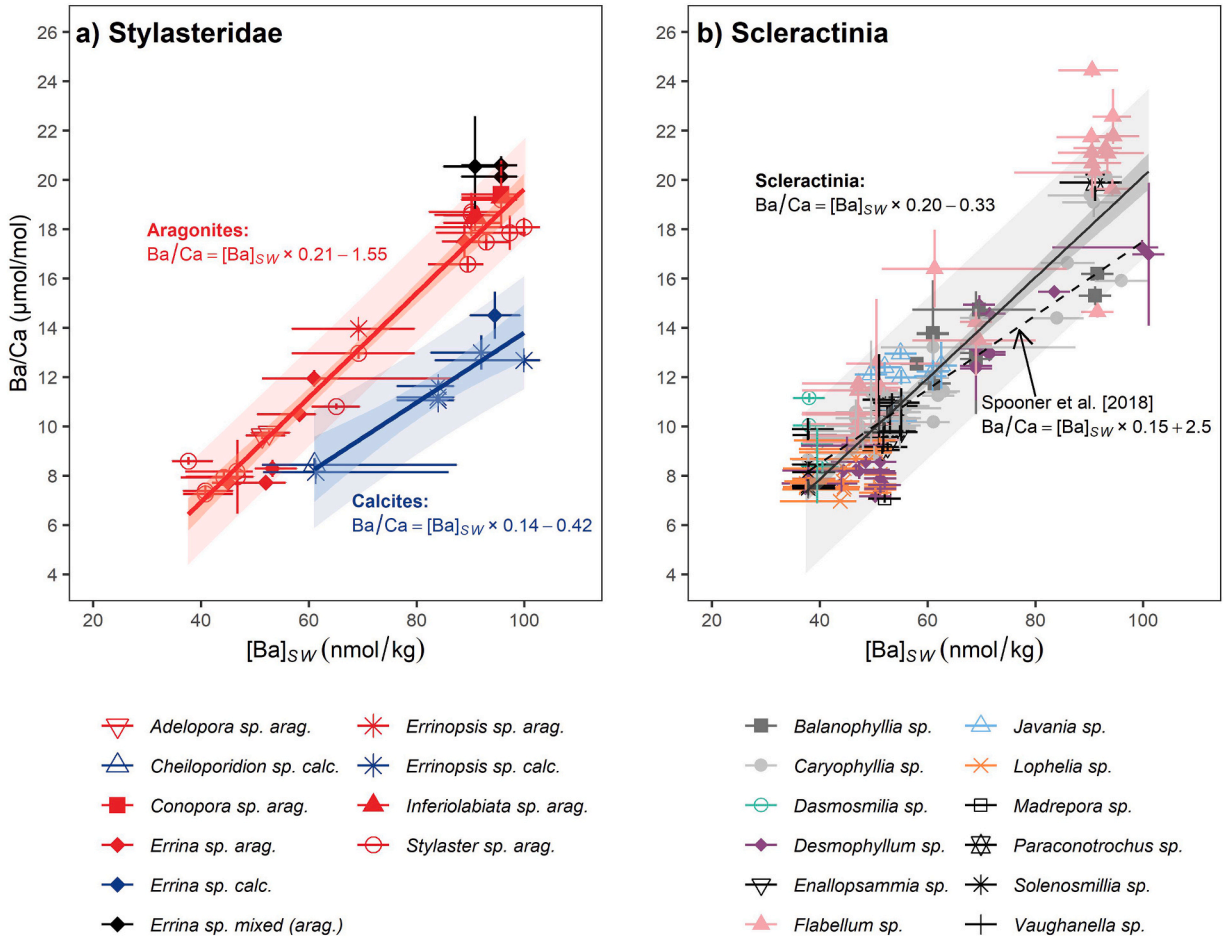


**Fig. 2.** a) Stylasterid Ba/Ca ratios plotted as a function of $[Ba]_{SW}$. b) Compiled scleractinian Ba/Ca ratios including samples from this study, Spooner et al. [2018] and Hemsing et al. [2018] plotted as a function of $[Ba]_{SW}$. Previous calibration from Spooner et al. [2018] is shown (black dashed line). Lines of best fit were calculated using Ordinary Least Squares regression, and exclude mixed mineralogy corals. Mixed mineralogy corals are composed of dominantly aragonite with minor high-Mg calcite. Dark shading represents 95% confidence intervals, lighter shading represents 95% prediction intervals. Horizontal error bars on data from this study show range of $[Ba]_{SW}$ measurements from the three closest profiles ± estimated analytical uncertainty. Vertical error bars are the largest of the analytical uncertainty or ± 2SD of replicate samples.

Ba/Ca ratios are less sensitive (shallower slope) to changes in $[Ba]_{SW}$ (Table 1). This difference is observed when comparing samples from the same genus (*Errina* sp. and *Errinopsis* sp.; Fig. 2a), and, crucially, those from the same collection locations and depths (e.g. compare aragonitic sample NBP1103-DH22-Stc1–01-Sde22aw ($D_{Ba}$ = 1.9) and calcitic sample NBP1103-DH22-Stc1–01-Efe22ax ($D_{Ba}$ = 1.3)). This strongly suggests these differences have a mineralogical origin, rather than being attributable to taxa- or location-specific variations in the calcification process (e.g. Mavromatis et al., 2018; Ulrich et al., 2021). Although mixed mineralogy stylasterids from the genus *Errina* have higher Ba/Ca than co-located, entirely aragonitic stylasterids (Fig. 3a), the reasons for this are likely specific to the species in question (Supplementary Information).

Mineralogical controls on $D_{Ba}$ of carbonate (bio)minerals are widely acknowledged (e.g. Mavromatis et al. 2018; Ulrich et al. 2021) and may also be reflected in other azooxanthellate coral taxa. This control is demonstrated by the similar $D_{Ba}$ values of aragonitic stylasterid and scleractinian corals, and of high-Mg calcitic stylasterid and bamboo corals, respectively (Fig. 3a). This similarity provides further support for a common process of Ba-incorporation into coral carbonate via cationic substitution (e.g. Anagnostou et al., 2011; LaVigne et al., 2011; LaVigne et al., 2016; Serrato Marks et al., 2017), and therefore suggests that $Ba^{2+}$ substitutes more easily into coralline aragonite than high-Mg calcite. Indeed, abiogenic precipitation experiments have shown that Ba incorporates more easily into aragonite than low-Mg calcite, due to the differing crystal structures of these two minerals (e.g. Mavromatis et al., 2018; Fig. 3b). However, high-Mg calcitic corals (LaVigne et al., 2011; Geyman et al., 2019; this study) have higher $D_{Ba}$ than low-Mg calcite produced by molluscs, planktonic foraminifera and in abiogenic precipitation experiments (e.g. Lea and Spero, 1994; Gillikin et al., 2006; Gillikin et al., 2008; Hönisch et al., 2011; Mavromatis et al., 2018; Ulrich et al., 2021; Fig. 3b). This could suggest that Ba-incorporation increases with Mg-content, due to increasing levels of lattice distortion (e.g. Mucci and Morse, 1983; Geyman et al., 2019).

An additional explanation for the difference between coral high-Mg calcite and low-Mg calcite is that Ba-incorporation is influenced by taxa-specific effects related to the calcification process (e.g. Mavromatis et al. 2018; Ulrich et al. 2021). Aragonitic coral (stylasterid and scleractinian) $D_{Ba}$ values are also elevated in comparison to aragonite produced by bivalves (Gillikin et al., 2008; Fig. 3b), fish (otoliths; Bath et al., 2000) and in some precipitation experiments (Mavromatis et al. 2018; Fig. 3b). This has led to suggestions that Ba-incorporation into coral carbonate is elevated by the coral calcification process (Mavromatis et al., 2018), and this hypothesis is explored in more detail in section 4.6. Identifying mineralogical controls on Ba-incorporation into marine carbonates by comparison of disparate calcifying taxa (e.g. Fig. 3b) is therefore difficult. Stylasterids, however, provide a phylogenetically-controlled natural mineralogical experiment, and our finding that mineralogy

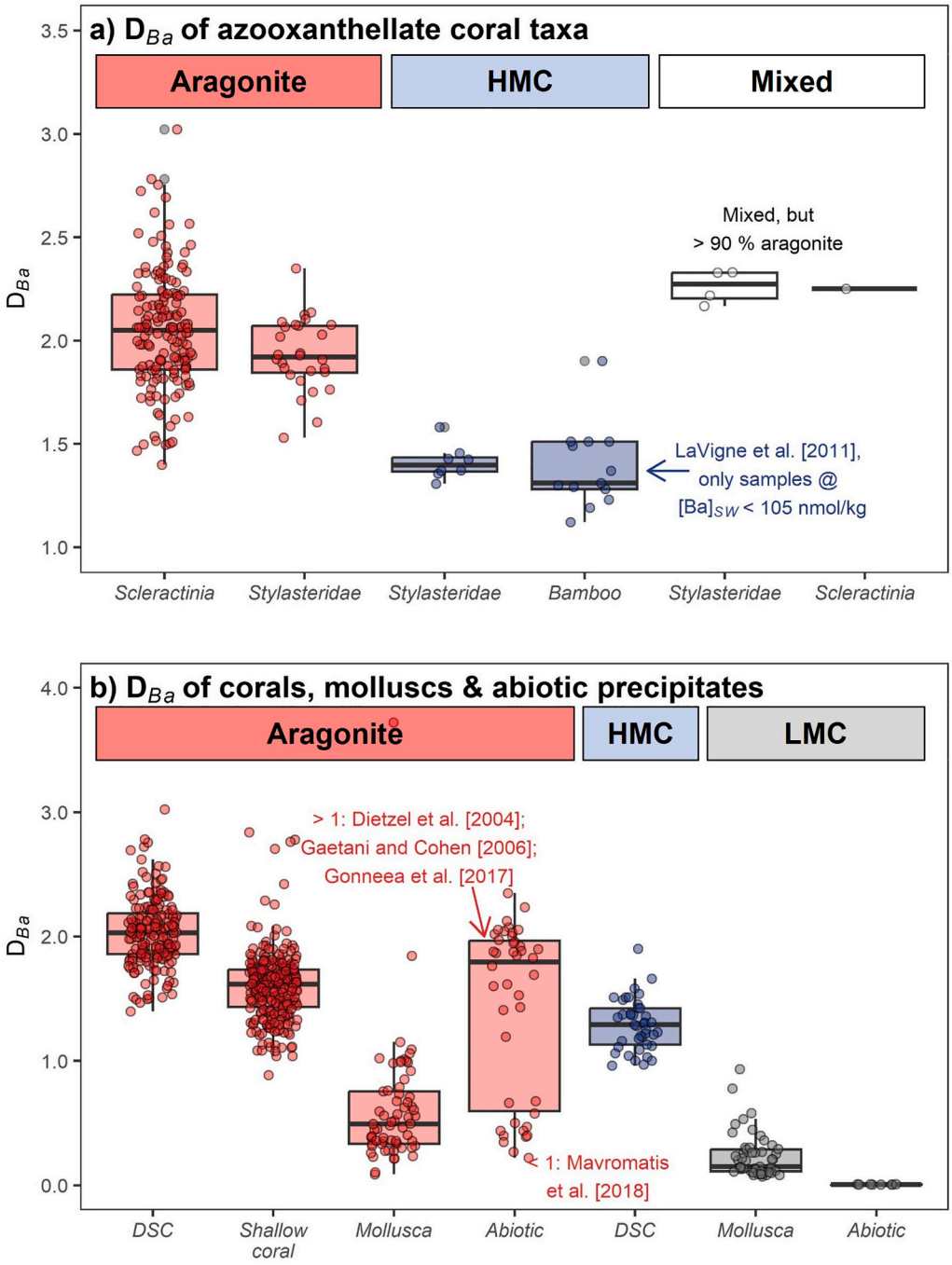


**Fig. 3.** Boxplots showing $D_{Ba}$ values of a) azooxanthellate coral taxa (this study; LaVigne et al., 2011 (only samples paired with $[Ba]_{SW}$ < 105 nmol/kg, see section 4.2 and Fig. 4); Hemsing et al., 2018; Spooner et al., 2018), and b) a wider range of marine calcifiers and abiotic precipitates, grouped by mineralogy (sources in Fig. 3a (including all samples from LaVigne et al., [2011]); Dietzel et al., 2004; Gaetani and Cohen, 2006; Gonneea et al., 2017; Mavromatis et al., 2018; Ulrich et al., 2021). Note change of scale between plots. DSC = deep-sea coral, HMC = high-Mg calcite, LMC = low-Mg calcite.

influences azooxanthellate coral Ba/Ca is robust. More broadly, this approach illustrates the utility of stylasterid skeletal geochemistry to deconvolve the environmental, mineralogical, and biological controls on the geochemistry of marine calcifiers (e.g. Ulrich et al., 2021).

### 4.2. Comparing azooxanthellate coral Ba/Ca vs $[Ba]_{SW}$ relationships

Ba/Ca vs $[Ba]_{SW}$ relationships have now been established for a range of azooxanthellate coral taxa. Comparing these reveals the dominant $[Ba]_{SW}$ and mineralogical controls on coral Ba/Ca (Fig. 4).

Our new high-Mg calcitic stylasterid relationship has a steeper gradient than the bamboo coral calibration published by LaVigne et al. [2011] (Table 1). This difference is driven by bamboo coral samples paired with higher $[Ba]_{SW}$ than our high-Mg calcitic stylasterid samples (LaVigne et al., 2011; Supplementary Information). These bamboo corals from deeper, Ba-enriched waters are impacted by decreasing $D_{Ba}$ with increasing water depth (Geyman et al. 2019). While we find no such relationship between our high-Mg calcitic stylasterid $D_{Ba}$ values and depth (Supplementary Information), our samples are generally from shallower depths, with only one sample from >1000 m. Directly comparing these datasets is therefore difficult, and considering data from the range of $[Ba]_{SW}$ represented in both studies (i.e. $[Ba]_{SW}$ < 105 nmol/kg only) reveals good agreement between the $D_{Ba}$ values and Ba/Ca vs $[Ba]_{SW}$ relationships of these two coral taxa (Fig. 3a; Fig. 4).

Similarly, aragonitic stylasterid and scleractinian Ba/Ca ratios are strongly related to $[Ba]_{SW}$, with similar slopes and similar average $D_{Ba}$ values (Fig. 3a; Fig. 4; Table 1; sections 3.1 and 3.2). While this suggests that $[Ba]_{SW}$ exerts a primary control on Ba/Ca ratios of both these coral

**Table 1**
Relationships between azooxanthellate coral Ba/Ca and $[Ba]_{SW}$ in the general form: Ba/Ca = m (± 2SE) × $[Ba]_{sw}$ + c (± 2SE). Results of both Ordinary Least Squares (OLS) and unweighted (orthogonal) Deming regression shown (see section 2.6). For stylasterids and Scleractinia, we recommend use of bold highlighted relationships when reconstructing past changes in $[Ba]_{SW}$. Prediction intervals calculated for Ba/Ca = 13 μmol/mol and 11 μmol/mol for aragonitic and calcitic calibrations, respectively. For details of regression types used and the meaning of statistical indicators, see section 2.6.

| Taxon | Source | *r* | *p* | Regression type | Gradient, m | (± 2SE) | Intercept, c | (± 2SE) | $r^2$ | 95% prediction interval |
|---|---|---|---|---|---|---|---|---|---|---|
| **Stylasterids (arag. all)** | **This study** | **0.98** | **< 0.05** | **OLS** | **0.21** | **0.02** | **−1.55** | **1.20** | **0.96** | **± 9.3** |
| | | | | Deming | 0.21 | 0.02 | −1.57 | 1.38 | – | |
| *Errina* sp. (arag.) | This study | 0.98 | < 0.05 | OLS | 0.24 | 0.05 | −3.83 | 3.20 | 0.96 | |
| *Stylaster* sp. (arag.) | This study | 0.98 | < 0.05 | OLS | 0.20 | 0.02 | −0.72 | 1.56 | 0.96 | |
| **Stylasterids (calc. all)** | **This study** | **0.94** | **< 0.05** | **OLS** | **0.14** | **0.04** | **−0.42** | **3.56** | **0.88** | **± 14.8** |
| | | | | Deming | 0.14 | 0.05 | −0.45 | 3.75 | – | |
| *Errinopsis* sp. (calc.) | This study | 0.96 | < 0.05 | OLS | 0.13 | 0.04 | 0.45 | 3.10 | 0.93 | |
| **Scleractinia (all)** | **This study;Spooner et al. [2018]; Hemsing et al. [2018]** | **0.90** | **< 0.05** | **OLS** | **0.20** | **0.02** | **−0.33** | **0.96** | **0.81** | **± 16.0** |
| | | | | Deming | 0.21 | 0.02 | −0.44 | 1.31 | – | |
| *Caryophyllia* sp. | This study; Spooner et al. [2018]; Hemsing et al. [2018] | 0.92 | < 0.05 | OLS | 0.18 | 0.02 | 1.02 | 1.51 | 0.85 | |
| *Desmophyllum* sp. | This study; Spooner et al. [2018]; Hemsing et al. [2018] | 0.95 | < 0.05 | OLS | 0.18 | 0.03 | 0.03 | 1.56 | 0.89 | |
| *Flabellum* sp. | This study; Spooner et al. [2018]; Hemsing et al. [2018] | 0.93 | < 0.05 | OLS | 0.23 | 0.04 | −0.24 | 2.74 | 0.87 | |
| Scleractinia | Spooner et al. [2018](included data from Hemsing et al. [2018]) | – | – | OLS | 0.15 | 0.02 | 2.5 | 1.4 | 0.7 | ± ~ 14 |
| Bamboo coral | LaVigne et al. [2011] | – | – | OLS | 0.079 | 0.008 | 4.205 | 0.870 | 0.77 | |

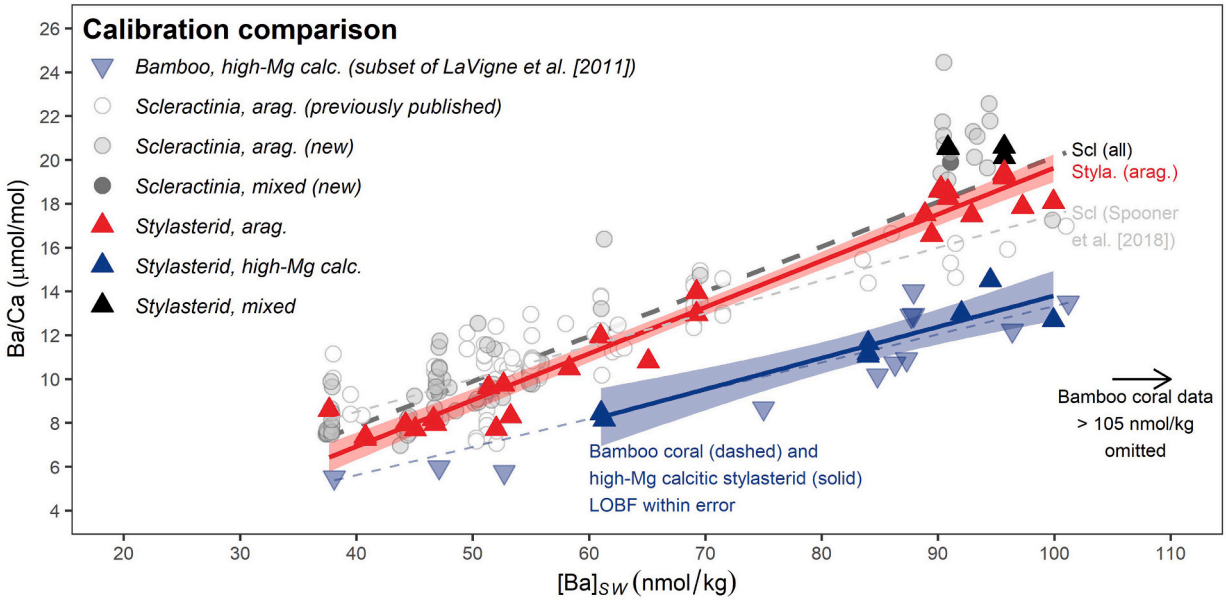


**Fig. 4.** Comparison of Ba/Ca vs $[Ba]_{SW}$ calibrations (Ordinary Least Squares) for different azooxanthellate coral groups, including Scleractinia (this study; Hemsing et al., 2018; Spooner et al., 2018), stylasterids (this study) and bamboo corals (LaVigne et al., 2011). Data from LaVigne et al. [2011] include only data points at $[Ba]_{SW}$ < 105 nmol/kg (see section 4.2). Error bars removed for clarity. Shading shows 95% confidence intervals.

taxa, more detailed comparison reveals important differences between them. Ba-incorporation into aragonitic stylasterid skeletons is less variable than into scleractinian skeletons, illustrated by the improved fit and narrower prediction interval of the regression between $[Ba]_{SW}$ and stylasterid Ba/Ca (Fig. 2; Table 1), the smaller variability of stylasterid $D_{Ba}$ values (mean 1.9 ± 0.4, 2SD) compared with Scleractinia (mean 2.0 ± 0.6, 2SD; Fig. 3a), and the smaller average difference between stylasterid sample replicates (Table 2). Additionally, our updated scleractinian Ba/Ca vs $[Ba]_{SW}$ relationship is significantly steeper than that reported previously (Spooner et al., 2018; Fig. 4), indicating that the addition of new samples has had a significant impact on the calibration.

These robust differences between stylasterid and scleractinian Ba/Ca ratios strongly suggest that contrasting secondary processes impact Ba-incorporation into their skeletons. In the following sections, we therefore examine the nature of these putative secondary controls, focusing firstly on stylasterids, then Scleractinia, before addressing the causes of the differences in Ba-incorporation between these two coral groups.

### 4.3. *Assessing the robustness of the stylasterid $[Ba]_{SW}$ proxy*

$[Ba]_{SW}$ and sample mineralogy exert primary controls on stylasterid Ba/Ca, suggesting this ratio may be a powerful archive of past $[Ba]_{SW}$. However, the possible influence of additional factors necessitates assessment of the reliability of stylasterids as archives of $[Ba]_{SW}$. In the

**Table 2**
Mean difference between Ba/Ca of replicates (different cut pieces) of corals analysed in this study. Averages for each taxon are also shown. Values >0.50 μmol/mol are shown in bold. For mixed mineralogy *Errina* sp. samples, between 2 and 6 replicates were measured on 3 corals, difference between maximum and minimum Ba/Ca values shown.

| Taxon | Genus | No. pairs | Mean difference Ba/Ca (μmol/mol) |
|---|---|---|---|
| *Scleractinia (all)* | – | 79 | 0.39 |
| | *Balanophyllia* sp. | 1 | 0.28 |
| | *Caryophyllia* sp. | 20 | 0.22 |
| | *Desmophyllum* sp. | 10 | 0.17 |
| | *Enallopsammia* sp. | 8 | 0.25 |
| | *Flabellum* sp. | 21 | 0.45 |
| | *Lophelia* sp.*(bulk calyx)* | 12 | **0.99** |
| | *Solenosmillia* sp. | 4 | 0.13 |
| | *Vaughanella* sp. | 3 | 0.17 |
| *Scleractinia (mixed)* | *Paraconotrochus* sp. *(mixed)* | 1 | **0.53** |
| *Stylasterid arag. (all)* | – | 28 | 0.26 |
| | *Adelopora* sp. | 2 | 0.05 |
| | *Conopora* sp. | 1 | **0.97** |
| | *Errina* sp. | 6 | 0.20 |
| | *Errinopsis* sp. | 1 | 0.04 |
| | *Inferiolabiata* sp. | 2 | 0.35 |
| | *Stylaster* sp. | 16 | 0.27 |
| *Stylasterid high-Mg calc. (all)* | – | 8 | 0.24 |
| | *Cheiloporidion* sp. | 1 | 0.20 |
| | *Errina* sp. | 1 | **0.68** |
| | *Errinopsis* sp. | 6 | 0.18 |
| *Stylasterid (mixed, arag.)* | *Errina* sp. | 3 corals | **1.42** |

following section, we investigate potential further influences on their Ba/Ca ratios, including genus-specific effects, a suite of additional hydrographic parameters, depth and location. Of these, only seawater temperature appears to influence stylasterid Ba/Ca, and the magnitude of this effect is small compared with the overriding $[Ba]_{SW}$ and mineralogical controls.

Our stylasterid sample set includes a range of genera, which could exhibit contrasting geochemical behaviour and influence our results. However, genus-specific relationships between Ba/Ca and $[Ba]_{SW}$ which span a substantial range in $[Ba]_{SW}$ are within error of the relationship for the full sample set (Table 1). This result suggests that our stylasterid relationships are not significantly biased by individual coral genera. We also find that most stylasterid genera display low variability between Ba/Ca of replicate samples (Table 2). *Conopora* sp. and *Errina* sp. *(calc.)* have relatively high variability, but these are based on one pair of replicates, while higher variability for mixed mineralogy stylasterids likely results from replicates incorporating variable amounts of each carbonate polymorph. This suggests that no single stylasterid genus measured here is significantly impacted by intra-skeletal variability in Ba/Ca, and all are suitable targets for use in reconstructing $[Ba]_{SW}$ using the bulk sampling methods employed here.

Secondly, we examine the residuals of our stylasterid Ba/Ca vs $[Ba]_{SW}$ relationships (i.e. $Ba/Ca_{measured} - Ba/Ca_{relationship}$) and stylasterid $D_{Ba}$ values to explore the influence of secondary environmental controls. These do not correlate with salinity, pH, $\Omega_{arag.}$, and dissolved phosphate concentrations ($p > 0.05$, $-0.28 < r < 0.35$; Supplementary Information). Additionally, while the residuals of the aragonitic calibration are significantly – but weakly – correlated with depth ($p = 0.02$, $r = -0.45$), similar correlations are not observed between depth and either the residuals of the calcitic calibration, or stylasterid $D_{Ba}$ ($p > 0.05$, $-0.32 < r < 0$; Supplementary Information). Furthermore, although aragonitic stylasterid $D_{Ba}$ values are significantly correlated with dissolved oxygen concentrations ($p = 0.04$, $r = 0.39$), a similar correlation is not observed for calcitic stylasterid $D_{Ba}$ values ($r = 0.08$) or for the residuals of the aragonitic or calcitic stylasterid calibrations ($p > 0.05$, $0 < r < 0.29$; Supplementary Information). Together, these results suggest that these parameters do not significantly influence Ba-incorporation into stylasterid skeletons. The strongest, consistent correlations for both aragonitic and calcitic stylasterid $D_{Ba}$ values are with temperature and dissolved silica concentrations (Fig. 5; Supplementary Information). Although neither temperature nor dissolved silica concentrations are significantly correlated with regression residuals (Supplementary Information), this does not preclude their influence on stylasterid Ba-incorporation. Both temperature and dissolved silica concentrations are strongly correlated with $[Ba]_{SW}$ in our dataset. This correlation with the x variable ($[Ba]_{SW}$) means that regression residuals will not reflect their possible influence in a straightforward manner. Instead, $D_{Ba}$ values are a better indicator of their possible effects, and the observed correlations suggest that one - or both - of these parameters may exert a secondary control on stylasterid skeletal Ba/Ca.

The tight negative correlation between temperature and dissolved silica concentration in our stylasterid sample set ($r = -0.88$) makes it difficult to isolate the effects of each variable. However, to our knowledge there is no published work examining the effects of dissolved silica concentration on Ba-incorporation into marine carbonates. Conversely, multiple experimental studies have shown that aragonite $D_{Ba}$ values are negatively correlated with ambient temperature (e.g. Dietzel et al., 2004; Gaetani and Cohen, 2006; Gonneea et al., 2017). Therefore, while we cannot discount that dissolved silica concentrations impact stylasterid $D_{Ba}$, we suggest that temperature is more likely the controlling variable. The strong correlation between temperature and dissolved silica concentration in our sample set could then lead to associated correlations between stylasterid $D_{Ba}$ and dissolved silica concentration.

Considering our stylasterid dataset more broadly, we find strong support for the role of temperature in Ba-incorporation into stylasterid skeletons. The $D_{Ba}$ of aragonite produced by abiotic precipitation experiments is also negatively correlated with temperature (Dietzel et al. 2004; Gaetani and Cohen 2006; Gonneea et al. 2017), and the gradients of the lines of best fit between stylasterid $D_{Ba}$ and temperature reported here are subparallel to that reported by Dietzel et al. [2004] for abiotic aragonite (Fig. 5a). Furthermore, a temperature effect can explain why aragonitic stylasterids collected from the cold waters of the Drake Passage and South Orkney regions have mean $D_{Ba}$ values of 1.96 (± 0.19, 2SD) and 2.09 (± 0.05, 2SD) respectively, higher than those from the comparatively warm equatorial (1.77 (± 0.29, 2SD)) and northeast (1.80 (± 0.10, 2SD)) Atlantic (Fig. 6b). Finally, a temperature influence can also explain the positive correlation between aragonitic stylasterid $D_{Ba}$ values and $[Ba]_{SW}$ (Fig. 6b). The negative covariation of temperature and $[Ba]_{SW}$ in the modern ocean means that colder waters tend to have higher $[Ba]_{SW}$ than warmer waters. Although we find no correlation between high-Mg calcitic stylasterid $D_{Ba}$ values and $[Ba]_{SW}$ (gradient = 0.001, $r = 0.14$), this may be attributable to the smaller temperature and $[Ba]_{SW}$ range represented in this dataset.

The mechanism by which temperature impacts stylasterid $D_{Ba}$ could relate to surface entrapment, whereby the temperature-dependent balance between crystal growth rate and element diffusivity impacts Ba-incorporation (e.g. Watson, 2004; Gaetani and Cohen, 2006). Alternatively, the biological response of the stylasterid calcification process to ambient temperature could lead to variations in Ba-incorporation due to kinetic effects or Rayleigh fractionation (Gaetani and Cohen 2006). As discussed in section 4.5, variations in Rayleigh fractionation appear to have a relatively small influence on stylasterid $D_{Ba}$. This may suggest that the surface entrapment model is the more likely cause, however this remains uncertain.

To constrain the magnitude of the temperature effect, we consider our aragonitic stylasterid sample set. Based on the correlation between aragonitic stylasterid $D_{Ba}$ and $[Ba]_{SW}$ in our sample set, $D_{Ba}$ increases by 11% as $[Ba]_{SW}$ increases from 40 to 100 nmol/kg (Fig. 6). Stylasterid Ba/Ca at the high (100 nmol/kg) $[Ba]_{SW}$ end of the relationship is therefore ~2 μmol/mol higher than the theoretical case in which $D_{Ba}$ remains constant at the value which characterises stylasterids at low (40 nmol/

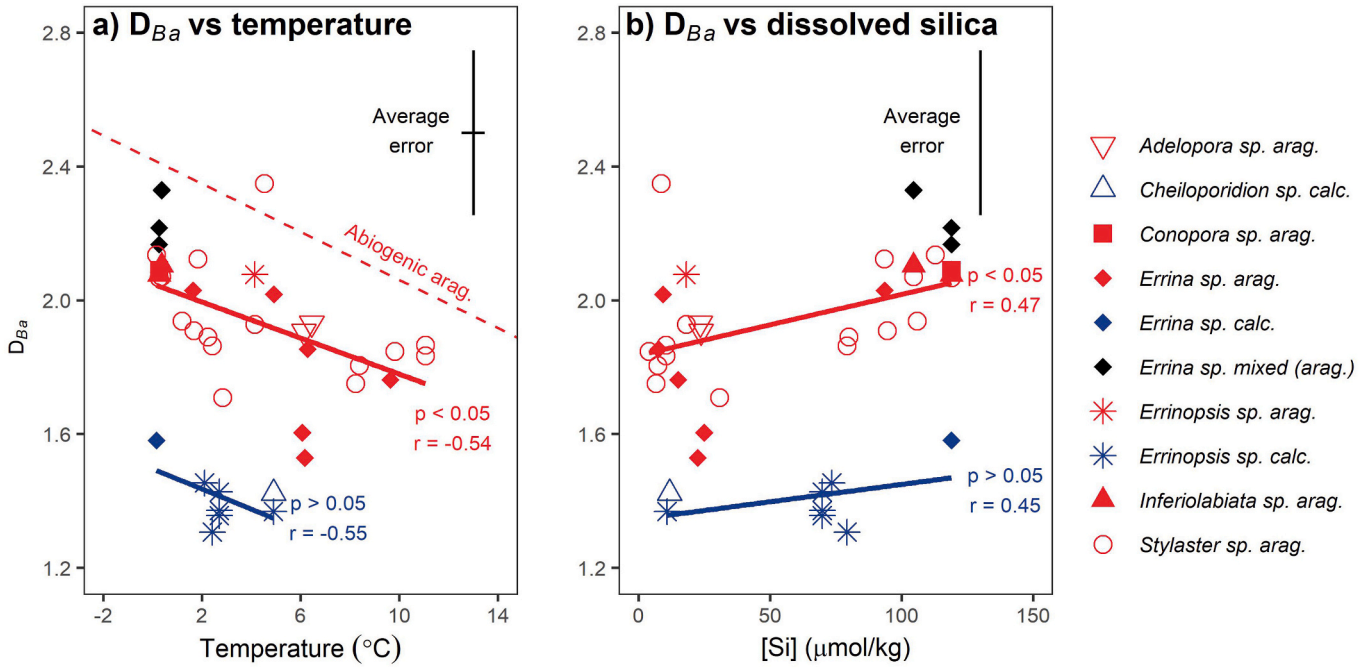


**Fig. 5.** Stylasterid $D_{Ba}$ values as a function of temperature (a) and dissolved silica concentration (b). Abiogenic aragonite vs temperature (dashed line) from Dietzel et al. [2004] also shown. Pearson r and *p*-values are shown for both aragonitic and calcitic stylasterids. Average error bars shown for data in this study, paucity of dissolved silica concentration data precludes x-error bar estimation in panel b.

kg) $[Ba]_{SW}$. Assuming this variation in $D_{Ba}$ is driven entirely by temperature, this suggests that temperature is responsible for ~16% of the overall variability in aragonitic stylasterid Ba/Ca. Therefore, while temperature does exert an influence on stylasterid Ba/Ca, these effects are minor compared with those caused by changes in $[Ba]_{SW}$, and are also smaller than those associated with sample mineralogy (average calcitic stylasterid $D_{Ba}$ 27% lower than aragonitic stylasterids). The small magnitude and uncertain nature of the temperature influence on stylasterid Ba/Ca (Fig. 5), coupled with the uncertainties in stylasterid temperature reconstruction (Stewart et al., 2020a; ± 2.3 °C using aragonitic stylasterid Li/Mg) mean that quantitatively correcting for this effect in palaeoceanographic contexts is unlikely to lead to more accurate estimates of past $[Ba]_{SW}$. Indeed, stylasterid Ba/Ca ratios are dominantly controlled by $[Ba]_{SW}$ and sample mineralogy, and provide a useful record of $[Ba]_{SW}$. Temporal records of stylasterid Ba/Ca should, however, ideally be presented alongside corresponding records of temperature-sensitive ratios (either Li/Mg, Sr/Ca or $\delta^{18}O$ (Samperiz et al. 2020; Stewart et al. 2020a)), allowing for qualitative assessment of whether changes in temperature might contribute to fluctuations in stylasterid Ba/Ca.

### 4.4. Secondary controls on scleractinian Ba/Ca

Previous work found that the secondary influences on scleractinian Ba/Ca ratios were minor (Spooner et al., 2018). However, as outlined in section 4.2, comparison of our expanded scleractinian dataset with aragonitic stylasterids reveals that scleractinian Ba/Ca ratios are characterised by as-yet-unexplained variability. We therefore reassess the potential influence of genus-specific effects, additional hydrographic parameters and location and depth on scleractinian Ba/Ca.

Our new scleractinian Ba/Ca vs $[Ba]_{SW}$ relationship includes samples from multiple genera, and relevant genus-specific relationships are within error of the full calibration (Table 1). However, the larger mean difference between scleractinian sample replicates - compared with aragonitic stylasterids – is driven mostly by two genera: *Lophelia* and *Flabellum* (Table 2). Considering *Lophelia*, our results are unsurprising given other heterogeneous aspects of their skeletal geochemistry (Raddatz et al., 2013; Montagna et al., 2014; Jurikova et al., 2019; Stewart et al., 2020a). The replicates measured here are samples of the entire *Lophelia* calyx, meaning Ba/Ca variability may be attributable to incorporation of skeletal centres of calcification (COCs) (Stewart et al., 2020a). To test this hypothesis, we also measured *Lophelia* samples taken only from theca walls, whose Li/Ca, Mg/Ca and Sr/Ca show smaller COC influence (see Stewart et al., 2020a, samples are same measured solutions). Theca-only subsamples have systematically lower Ba/Ca than bulk calyx samples by around 10% (Supplementary Information). In zooxanthellate Scleractinia, COCs have elevated Ba/Ca compared to the rest of the skeleton (Holcomb et al., 2009), therefore our result may be consistent with decreased incorporation of COC material into theca-only subsamples, compared with the bulk calyx. Careful sampling of *Lophelia* theca apparently mitigates some of the effects of COC incorporation, and we use these theca-only subsamples in our Ba/Ca vs $[Ba]_{SW}$ relationship where available.

Equally, *Flabellum* sp. is prone to particularly high and variable Ba/Ca (Fig. 2b). Previous studies have concluded that other aspects of the skeletal geochemistry of *Flabellum* sp., including Li/Mg (Case et al., 2010; Cuny-Guirriec et al., 2019; Stewart et al., 2020a), Sr/Ca, $\delta^{18}O$ and $\delta^{13}C$ (Stewart et al., 2020a), are not unusual in comparison to other azooxanthellate scleractinian genera. However, multiple studies have recorded *Flabellum* from substrates dominated by fine muds and sands (e.g. Buhl-Mortensen et al., 2007; Hamel et al., 2010; Mercier et al., 2011), and some *Flabellum* species are also free-living, lying sideways in direct contact with sediment (Hamel et al. 2010; Mercier et al. 2011). This habitat may result in *Flabellum* samples experiencing higher $[Ba]_{SW}$ due to barium efflux from sediments into the water column (e.g. McManus et al., 1994; Hoppema et al., 2010; Bates et al., 2017). Additionally, this proximity to sediment may mean that *Flabellum* is particularly susceptible to contamination by Ba-bearing phases such as barite and/or Fe—Mn oxyhydroxides. Indeed, three of the six scleractinian corals which had Ba/Ca data excluded due to high Fe/Ca were *Flabellum* (Supplementary Information). However, Ba-incorporation into *Flabellum* does not differ significantly from other scleractinian genera or our overall Ba/Ca vs $[Ba]_{SW}$ relationship (Table 1). Therefore, we retain this genus in our Ba/Ca vs $[Ba]_{SW}$ relationship, but emphasise the

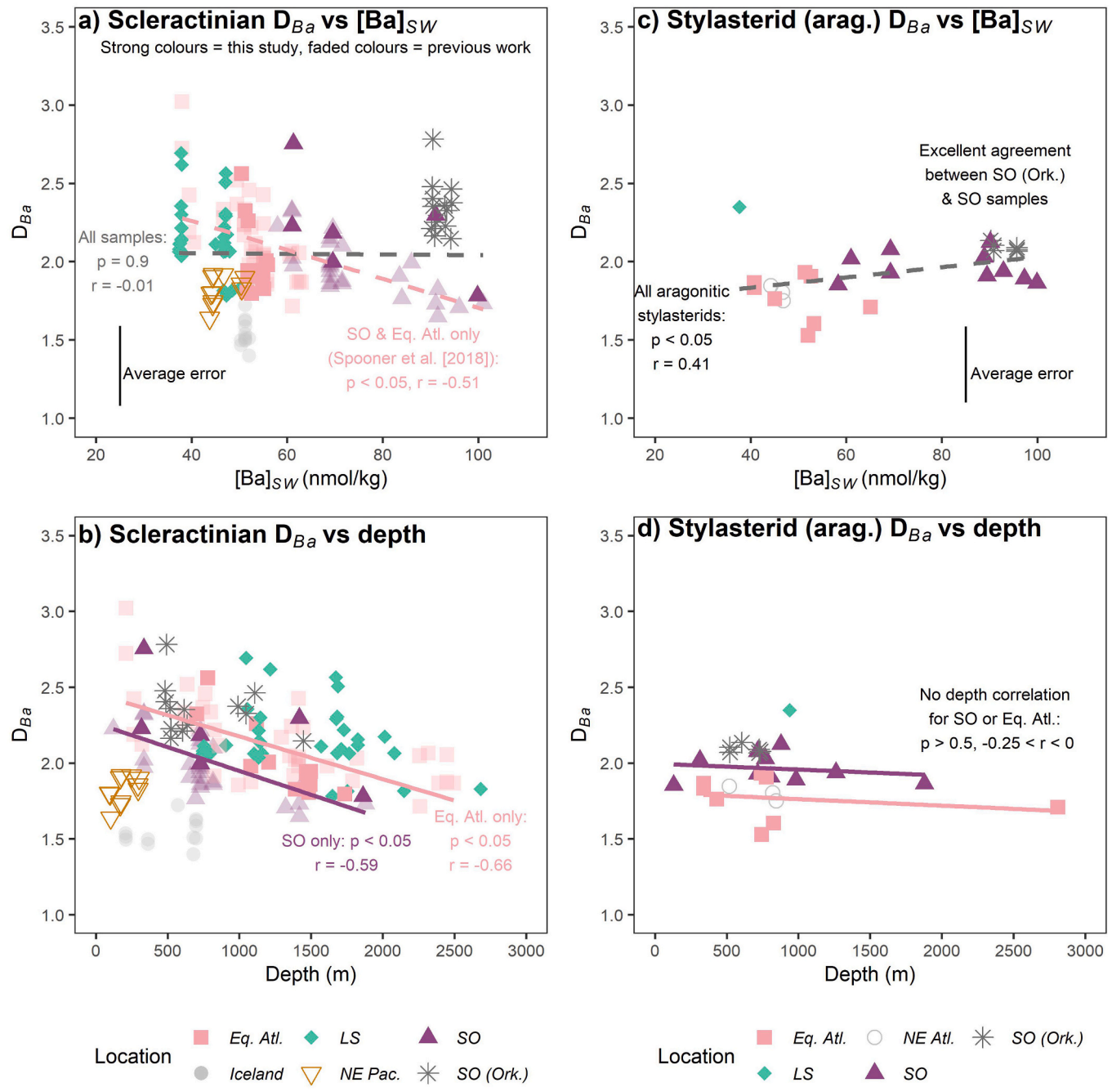


**Fig. 6.** Scleractinian (a) and aragonitic stylasterid (b) $D_{Ba}$ values as a function of $[Ba]_{SW}$, by location. Location codes follow Fig. 1. Average vertical error bars shown in panels a and c.

importance of screening samples for contaminant phases.

Although genus-specific effects may account for the larger average difference between Ba/Ca of scleractinian coral replicates compared with aragonitic stylasterids, they cannot explain the overall higher variability in scleractinian $D_{Ba}$, or worse fit of the scleractinian Ba/Ca vs $[Ba]_{SW}$ relationship. Instead, we suggest that Ba-incorporation in scleractinian corals varies between locations, and across depth gradients. Previous work has shown that Icelandic Scleractinia have lower $D_{Ba}$ values than those collected from the equatorial Atlantic and Southern Ocean (Hemsing et al., 2018; Spooner et al., 2018; Fig. 6a). Our new data show that Scleractinia from the northeast Pacific (NE Pac.) region also have low $D_{Ba}$, while those from South Orkney (SO Ork) and Labrador Sea (LS) sites have high $D_{Ba}$ (Fig. 6a). These samples steepen the gradient of our scleractinian Ba/Ca vs $[Ba]_{SW}$ relationship relative to that published previously, and erode the relationship between scleractinian $D_{Ba}$ and $[Ba]_{SW}$ (Spooner et al., 2018, their fig. 10). Locational differences become increasingly apparent when $D_{Ba}$ values are considered as a function of water depth: Scleractinia from the Drake Passage and equatorial Atlantic regions show sub-parallel, negative correlations between $D_{Ba}$ and water depth ($r = -0.59$ and -0.66, respectively, $p < 0.05$; Fig. 6b). Because $[Ba]_{SW}$ increases with increasing water depth in the modern ocean, a depth control on scleractinian $D_{Ba}$ in these two regions may explain the correlation observed between scleractinian $D_{Ba}$ and $[Ba]_{SW}$ when considering these two regions in isolation (Fig. 6; Spooner et al., 2018, their fig. 10).

No single variable can explain both the location and depth-related variability in scleractinian $D_{Ba}$ values. While the decrease in scleractinian $D_{Ba}$ values with increasing water depth may be explained by

partition coefficients approaching unity as pressure increases (McCorkle et al., 1995), this cannot explain locational differences. We also find no strong correlations between any of the ancillary hydrographic variables considered here and either scleractinian $D_{Ba}$ values or residuals of the Ba/Ca vs $[Ba]_{SW}$ relationship ($-0.20 < r < 0.20$; Supplementary Information). The only significant correlation found is between scleractinian calibration residuals and temperature ($p = 0.03$, $r = -0.17$). However, this correlation is weak, and temperature does not correlate significantly with scleractinian $D_{Ba}$ values ($p > 0.05$, $r = -0.15$). These results suggest that none of these additional hydrographic properties exert a dominant influence on scleractinian Ba-incorporation, in agreement with previous work (Anagnostou et al., 2011; Hemsing et al., 2018; Spooner et al., 2018). Crucially, aragonitic stylasterids from the same sites show less locational variability and no correlations with water depth (Fig. 6). This suggests the driver of the variability in scleractinian $D_{Ba}$ is specific to Scleractinia, and affects stylasterid Ba/Ca to a lesser degree.

Therefore, we suggest that depth trends and geographic differences result from the scleractinian calcification process (Spooner et al. 2018). In the following section, we consider two main mechanisms which could cause calcification-related variability in scleractinian Ba/Ca: variations in the degree of Rayleigh fractionation (i.e., the relative rates of coral growth and calcifying fluid replenishment; Gaetani and Cohen, 2006; Pretet et al., 2015; Geyman et al., 2019; Reed et al., 2021), and the precipitation of witherite ($BaCO_3$) within the domains of aragonite (Mavromatis et al., 2018; Liu et al., 2019).

### 4.5. Comparing scleractinian and stylasterid calcification processes

Comparing Ba/Ca and Sr/Ca ratios of stylasterid and scleractinian corals suggests that variations in the degree of Rayleigh fractionation is the most likely cause of the increased variability in scleractinian $D_{Ba}$. The (partial) isolation of the scleractinian calcifying fluid means that Rayleigh fractionation processes can affect the composition of the coral skeleton (e.g. Gaetani and Cohen, 2006; Gagnon et al., 2007). Because coral $D_{Ba} > 1$, barium is preferentially incorporated into the skeleton during growth, and becomes progressively depleted in the calcifying fluid. The rate of skeletal growth relative to the timescale of calcifying fluid replenishment – precipitation efficiency – thus affects how much Ba is ultimately incorporated into the coral skeleton. Indeed, Rayleigh fractionation has been suggested to affect Ba-incorporation into zooxanthellate Scleractinia (Gaetani and Cohen, 2006; Pretet et al., 2015; Reed et al., 2021) and azooxanthellate bamboo corals (Geyman et al., 2019). In this framework, decreasing $D_{Ba}$ with increasing depth suggests that Scleractinia calcify more efficiently in deeper waters, and most efficiently in Icelandic waters, compared to other locations.

To test this hypothesis, we compare Ba/Ca data with Sr/Ca ratios measured on the same samples (same solutions; Fig. 7). Stylasterid Sr/Ca ratios are sensitive to temperature, while scleractinian Sr/Ca ratios show the combined influence of temperature and Rayleigh fractionation (Gagnon et al., 2007; Ross et al., 2019; Stewart et al., 2020a; Supplementary Information). The effects of Rayleigh fractionation should in turn be reflected in the residuals of the scleractinian Sr/Ca – temperature relationship (Ross et al., 2019; Stewart et al., 2020a), and should result in a positive correlation between Sr/Ca-temperature residuals and $D_{Ba}$ because both $D_{Sr}$ and $D_{Ba}$ of coral aragonite are greater than 1 (Gaetani and Cohen, 2006).

Although both aragonitic stylasterid and scleractinian $D_{Ba}$ values are positively correlated with Sr/Ca ratios ($p < 0.05$, $r > 0.61$; Fig. 7), we find an insignificant and comparatively weak correlation between aragonitic stylasterid $D_{Ba}$ and Sr/Ca-temperature residuals ($p = 0.07$, $r = 0.35$; Fig. 7c). This strongly suggests that temperature is driving the covariance between stylasterid $D_{Ba}$ and Sr/Ca (see section 4.3), and that variations in the degree of Rayleigh fractionation between stylasterid coral samples are small. Conversely, our scleractinian $D_{Ba}$ values retain a significant, positive correlation with Sr/Ca-temperature residuals ($p < 0.05$, $r = 0.55$; Fig. 7b), supporting the hypothesis that Rayleigh fractionation impacts Sr- and Ba-incorporation into scleractinian skeletons.

Variations in the degree of Rayleigh fractionation may explain variability in scleractinian $D_{Ba}$ between locations and across depth gradients, as well as the absence of a dominant environmental control on scleractinian $D_{Ba}$ (section 4.4). This is because scleractinian growth rates and the degree of isolation of the calcifying fluid are likely to be affected by a range of variables including food supply (e.g. Crook et al., 2013; Büscher et al., 2017), oxygen concentrations, carbonate system parameters and temperature (e.g. Büscher et al., 2017; Gómez et al., 2018), which in turn vary between locations and with depth. For example, decreasing $D_{Ba}$ with increasing depth suggests that Scleractinia calcify more efficiently in deeper waters, either growing more quickly or employing greater isolation of their calcifying fluid, as previously suggested for bamboo corals (Geyman et al. 2019). Given that pH, oxygen concentration and food supply all tend to decrease with increasing depth in the ocean, it seems unlikely that coral growth rate would increase with increasing depth, and instead more efficient calcification with depth may result from increasing isolation of the scleractinian calcifying fluid (e.g. Geyman et al., 2019). Equally, Scleractinia from Iceland and the northeast Pacific apparently calcify more efficiently than those from other regions, perhaps due to high growth rates during intense seasonal peaks in primary productivity (and thus food supply) in these regions (e.g. see data in Sathyendranath et al., 2019; Sathyendranath et al., 2021). Although we cannot isolate the controlling variable(s), Rayleigh fractionation provides a plausible explanation for the variability in scleractinian $D_{Ba}$.

A second hypothesis for the cause of variability in scleractinian $D_{Ba}$ is the incorporation of witherite ($BaCO_3$) into the coral skeleton during growth (Mavromatis et al., 2018), which may affect Ba/Ca ratios of zooxanthellate Scleractinia (Liu et al. 2019). It is well-established that scleractinian corals heavily modify their calcifying fluid, increasing pH and $[CO_3]^{2-}$ (and therefore $\Omega_{arag.}$) to promote calcification (Al-Horani et al., 2003; Sinclair and Risk, 2006). At high degrees of carbonate oversaturation, coprecipitation of witherite ($BaCO_3$) within the domain of aragonite is likely, but is supressed at lower degrees of oversaturation (Mavromatis et al. 2018). Therefore, variations in the carbonate chemistry of the scleractinian calcifying fluid could lead to variations in witherite formation and, consequently, coral $D_{Ba}$.

However, Sr/Ca ratios should be unaffected by witherite precipitation, meaning this hypothesis cannot explain the observed correlation between scleractinian Sr/Ca-temperature residuals and $D_{Ba}$ (Fig. 7b). Additionally, comparing stylasterids and Scleractinia challenges the notion that the amount of witherite precipitation is particularly sensitive to fluctuations in the carbonate chemistry of the coral calcifying fluid. Stylasterid skeletal $\delta^{11}B$, U/Ca and B/Ca suggest that stylasterids calcify from a fluid with significantly lower pH, $[CO_3]^{2-}$ and $\Omega_{arag.}$ than Scleractinia (Stewart et al., 2022). Therefore, if witherite precipitation were responding to variations in calcifying fluid carbonate chemistry, we would expect stylasterids to have consistently lower $D_{Ba}$ values than Scleractinia. Yet, the average $D_{Ba}$ values of these coral taxa are very similar (Fig. 3a), implying that comparatively small variations in the carbonate chemistry of the scleractinian calcifying fluid are unlikely to lead to substantial differences in witherite precipitation.

Therefore, we suggest that varying degrees of Rayleigh fractionation, perhaps in response to environmental conditions, are the most likely cause of variability in scleractinian Ba/Ca ratios. Conversely, stylasterid Ba/Ca ratios are less variable, suggesting either they are not affected by Rayleigh fractionation, or that the relative rates of stylasterid growth and calcifying fluid isolation are comparatively invariant across a range of ocean conditions. This adds to the growing evidence for contrasting biomineralisation mechanisms in stylasterid and scleractinian corals, with recent work showing that stylasterid Li/Mg, Sr/Ca, $\delta^{18}O$, $\delta^{13}C$ and $\delta^{11}B$ are also less impacted by calcification-related effects than these same ratios in Scleractinia (Samperiz et al., 2020; Stewart et al., 2020a; Stewart et al., 2022).

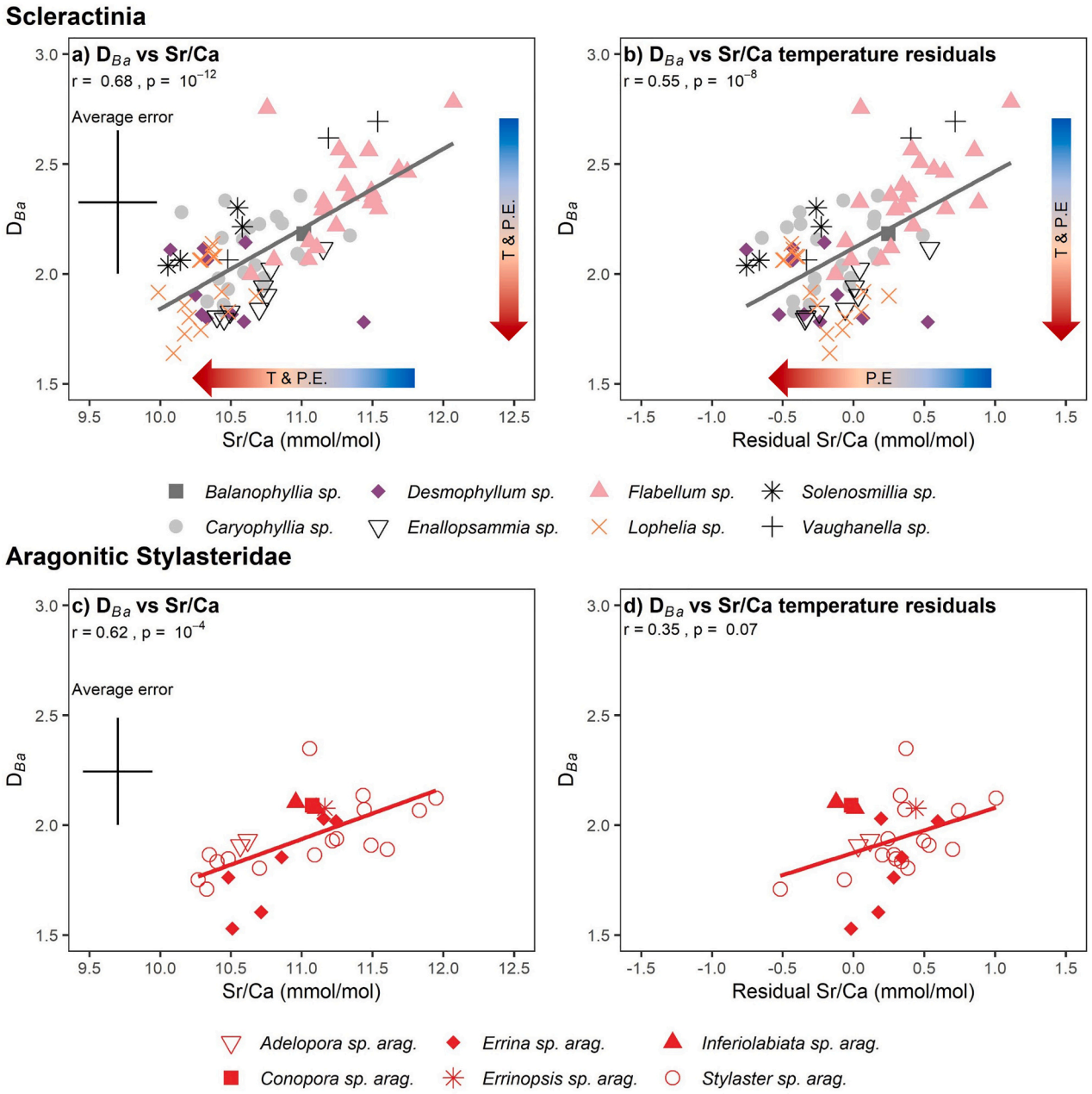


**Fig. 7.** Scleractinian (top) and aragonitic stylasterid (bottom) $D_{Ba}$ values as a function of Sr/Ca (a & c) and Sr/Ca temperature residuals (b & d; residuals = $Sr/Ca_{coral}$ - $Sr/Ca_{calibration}$). Effect of increasing temperature (T) and precipitation efficiency (P.E.) on Sr/Ca and $D_{Ba}$ indicated in a and b. Average error bars shown in panels a and c. Sr/Ca error bars are the largest of the analytical uncertainty or ± 2SD of replicate samples. The mixed mineralogy scleractinian *Paraconotrochus* sp. was not included in these plots.

### 4.6. *Implications for elevated coral $D_{Ba}$*

The differences between stylasterid and scleractinian coral calcification may have important implications for understanding why $D_{Ba}$ values of a range of coral taxa are - for a given mineralogy - both similar to one another, and elevated compared to other marine calcifiers and experimentally-produced carbonates (section 4.1; Fig. 3).

While abiogenic aragonite with $D_{Ba} > 1$ has been produced by some precipitation experiments (Dietzel et al., 2004; Gaetani and Cohen, 2006; Gonneea et al., 2017; Fig. 3b), this has recently been attributed to the influence of witherite at high aragonite saturation states, and pure aragonite produced at lower degrees of carbonate saturation ($\Omega_{arag.} < 2$) has $D_{Ba}$ less than 1 (Mavromatis et al., 2018; Fig. 3b). Therefore, it has been suggested that witherite precipitation in the domains of aragonite could also be responsible for elevated coral $D_{Ba}$ compared with other marine calcifiers (Mavromatis et al. 2018). However, the similarity of stylasterid and scleractinian $D_{Ba}$ values challenges this idea. As outlined above, while Scleractinia are known to calcify from a fluid which is highly oversaturated with respect to carbonate (Al-Horani et al. 2003; Sinclair and Risk 2006), stylasterids are thought to calcify from a fluid with $\Omega_{arag.} \sim 1.5$ (Stewart et al. 2022). Therefore, although stylasterid and scleractinian corals share similar average $D_{Ba}$, they likely form their skeletons from fluids with very different degrees of carbonate oversaturation. In turn, this may indicate that elevated coral $D_{Ba}$ does not result from witherite precipitation triggered by high degrees of carbonate oversaturation in the coral calcifying fluid.

These estimates of stylasterid calcifying fluid $\Omega_{arag.}$ are minimum estimates, and it is possible that a small degree of additional pH and

$\Omega_{arag.}$ upregulation occurs (Stewart et al. 2022), which may exceed the threshold for witherite precipitation. In this sense, consistent amounts of witherite precipitation above its saturation threshold could cause consistent elevation in stylasterid and scleractinian coral $D_{Ba}$. Alternatively, enrichment in coral Ba/Ca may instead result from precipitation of amorphous carbonate phases (Mavromatis et al. 2018), or the presence of organic molecules which act as templates for calcification (e.g. Drake et al., 2021) and can influence skeletal composition (e.g. Mavromatis et al., 2017; Mavromatis et al., 2018). Although we cannot constrain the reasons for the enrichment in coral $D_{Ba}$ here, our data clearly illustrate that explanations for elevated Ba-incorporation into coral carbonate need to consider the diversity of coral calcification mechanisms.

## 5. Conclusions

We present the first measurements of stylasterid skeletal Ba/Ca ratios. Mineralogy exerts a strong control on stylasterid Ba/Ca, with aragonitic samples having higher Ba/Ca than their high-Mg calcitic counterparts. However, when each mineralogy is considered separately, stylasterid skeletal Ba/Ca ratios are strongly, linearly correlated with $[Ba]_{SW}$. We find that temperature exerts a secondary control on Ba-incorporation into stylasterid skeletons, consistent with abiogenic precipitation experiments. Simultaneous measurement of temperature sensitive Li/Mg and/or Sr/Ca ratios in stylasterid samples provides a means to qualitatively assess the possible role of temperature in palaeoceanographic $[Ba]_{SW}$ records.

Azooxanthellate scleractinian Ba/Ca ratios are more sensitive to changes in $[Ba]_{SW}$ than previously thought (Spooner et al., 2018), driven by differences in Ba-incorporation between locations and across depth gradients. Paired Ba/Ca and Sr/Ca values are consistent with the influence of Rayleigh fractionation related to the coral calcification process. The driver(s) of this process remains unclear, likely due to the competing influence of multiple oceanographic parameters on the scleractinian calcification process. Crucially, stylasterid skeletal Ba/Ca ratios are impacted less by calcification processes, and with robust $[Ba]_{SW}$ and temperature proxies now established (Samperiz et al., 2020; Stewart et al., 2020a), stylasterid corals are a valuable multi-proxy palaeoceanographic archive.

## Funding

Funding for this work was provided by a NERC GW4+ Doctoral Training Partnership (NE/S007504/1) studentship awarded to J.K., an Antarctic Bursary awarded to J.A.S, and NERC grants awarded to L.F.R. (NE/S001743/1; NE/R005117/1; NE/N003861/1; NE/X00127X/1). Cruise DY081 was funded by European Research Council starting grant ICY-LAB (Grant Agreement 678371).

## Declaration of Competing Interest

The authors declare that they have no known competing financial interests or personal relationships that could have appeared to influence the work reported in this paper.

## Data availability

All new Ba/Ca, Sr/Ca, Fe/Ca and Mn/Ca data are included in the supplementary data tables, along with detailed coral information and paired hydrographic data. The supplementary data tables also contain compiled (this study and previous work) Ba/Ca vs $[Ba]_{SW}$ data for azooxanthellate Scleractinia, and compiled (this study and previous work) Sr/Ca vs temperature data for stylasterid and scleractinian azooxanthellate corals.

## Acknowledgements

We acknowledge and thank the crew and researchers on board the research vessels that obtained the samples for this study, and would like to thank Veerle Huvenne for access to the sample from cruise CE14001. We are grateful to Chris Coath, Carolyn Taylor, and Emily Ciscato for their help with laboratory work.

## Appendix A. Supplementary data

Supplementary data to this article can be found online at https://doi.org/10.1016/j.chemgeo.2023.121355.

## References

GEOTRACES Intermediate Data Product Group, 2021. The GEOTRACES Intermediate Data Product 2021 (IDP2021). NERC EDS British Oceanographic Data Centre NOC. https://doi.org/10.5285/cf2d9ba9-d51d-3b7c-e053-8486abc0f5fd.

Al-Horani, F.A., Al-Moghrabi, S.M., de Beer, D., 2003. Microsensor study of photosynthesis and calcification in the scleractinian coral, *Galaxea fascicularis*: active internal carbon cycle. J. Exp. Mar. Biol. Ecol. 288, 1–15. https://doi.org/10.1016/S0022-0981(02)00578-6.

Anagnostou, E., Sherrell, R.M., Gagnon, A., LaVigne, M., Field, M.P., McDonough, W.F., 2011. Seawater nutrient and carbonate ion concentrations recorded as P/Ca, Ba/Ca, and U/ca in the deep-sea coral *Desmophyllum dianthus*. Geochim. Cosmochim. Acta 75, 2529–2543. https://doi.org/10.1016/j.gca.2011.02.019.

Barker, S., Greaves, M., Elderfield, H., 2003. A study of cleaning procedures used for foraminiferal Mg/Ca paleothermometry. Geochem. Geophys. Geosyst. 4.(9) https://doi.org/10.1029/2003GC000559.

Bates, S., 2016. Barium Uptake by Foraminifera: Understanding Past and Present Ocean Processes. Doctoral dissertation,. University of Bristol.

Bates, S.L., Hendry, K.R., Pryer, H.V., Kinsley, C.W., Pyle, K.M., Woodward, E.M.S., Horner, T.J., 2017. Barium isotopes reveal role of ocean circulation on barium cycling in the Atlantic. Geochim. Cosmochim. Acta 204, 286–299. https://doi.org/10.1016/j.gca.2017.01.043.

Bath, G.E., Thorrold, S.R., Jones, C.M., Campana, S.E., McLaren, J.W., Lam, J.W.H., 2000. Strontium and barium uptake in aragonitic otoliths of marine fish. Geochim. Cosmochim. Acta 64, 1705–1714. https://doi.org/10.1016/S0016-7037(99)00419-6.

Bishop, J.K.B., 1988. The barite-opal-organic carbon association in oceanic particulate matter. Nature 332, 341–343. https://doi.org/10.1038/332341a0.

Boyle, E.A., 1981. Cadmium, zinc, copper, and barium in foraminifera tests. Earth Planet. Sci. Lett. 53, 11–35. https://doi.org/10.1016/0012-821X(81)90022-4.

Buhl-Mortensen, L., Mortensen, P.B., Armsworthy, S., Jackson, D., 2007. Field observations of *Flabellum spp.* and laboratory study of the behavior and respiration of *Flabellum alabastrum*. Bull. Mar. Sci. 81, 543–552.

Büscher, J.V., Form, A.U., Riebesell, U., 2017. Interactive effects of ocean acidification and warming on growth, fitness and survival of the cold-water coral *lophelia pertusa* under different food availabilities. Front. Mar. Sci. 4, 101. https://doi.org/10.3389/fmars.2017.00101.

Cairns, S.D., 2007. Deep-water corals: an overview with special reference to diversity and distribution of deep-water scleractinian corals. Bull. Mar. Sci. 81, 311–322.

Cairns, S.D., 2011. Global Diversity of the Stylasteridae (Cnidaria: Hydrozoa: Athecatae). PLoS One 6, e21670. https://doi.org/10.1371/journal.pone.0021670.

Cairns, S.D., Macintyre, I.G., 1992. Phylogenetic Implications of Calcium Carbonate Mineralogy in the Stylasteridae (Cnidaria: Hydrozoa). PALAIOS 7, 96. https://doi.org/10.2307/3514799.

Case, D.H., Robinson, L.F., Auro, M.E., Gagnon, A.C., 2010. Environmental and biological controls on Mg and Li in deep-sea scleractinian corals. Earth Planet. Sci. Lett. 300, 215–225. https://doi.org/10.1016/j.epsl.2010.09.029.

Chan, L.H., Drummond, D., Edmond, J.M., Grant, B., 1977. On the barium data from the Atlantic GEOSECS expedition. Deep-Sea Res. 24, 613–649. https://doi.org/10.1016/0146-6291(77)90505-7.

Collier, R., Edmond, J., 1984. The trace element geochemistry of marine biogenic particulate matter. Prog. Oceanogr. 13, 113–199. https://doi.org/10.1016/0079-6611(84)90008-9.

Crook, E.D., Cooper, H., Potts, D.C., Lambert, T., Paytan, A., 2013. Impacts of food availability and $pCO_2$ on planulation, juvenile survival, and calcification of the azooxanthellate scleractinian coral *Balanophyllia elegans*. Biogeosciences 10, 7599–7608. https://doi.org/10.5194/bg-10-7599-2013.

Cuny-Guirriec, K., Douville, E., Reynaud, S., Allemand, D., Bordier, L., Canesi, M., Mazzoli, C., Taviani, M., Canese, S., McCulloch, M., Trotter, J., Rico-Esenaro, S.D., Sanchez-Cabeza, J.-A., Ruiz-Fernández, A.C., Carricart-Ganivet, J.P., Scott, P.M., Sadekov, A., Montagna, P., 2019. Coral Li/Mg thermometry: Caveats and constraints. Chem. Geol. 523, 162–178. https://doi.org/10.1016/j.chemgeo.2019.03.038.

Dehairs, F., Chesselet, R., Jedwab, J., 1980. Discrete suspended particles of barite and the barium cycle in the open ocean. Earth Planet. Sci. Lett. 49, 528–550. https://doi.org/10.1016/0012-821X(80)90094-1.

Dickinson, S.R., McGrath, K.M., 2001. Quantitative determination of binary and tertiary calcium carbonate mixtures using powder X-ray diffraction. Analyst 126, 1118–1121. https://doi.org/10.1039/b103004n.

Dietzel, M., Gussone, N., Eisenhauer, A., 2004. Co-precipitation of $Sr^{2+}$ and $Ba^{2+}$ with aragonite by membrane diffusion of $CO_2$ between 10 and 50 °C. Chem. Geol. 203, 139–151. https://doi.org/10.1016/j.chemgeo.2003.09.008.

Drake, J.L., Varsano, N., Mass, T., 2021. Genetic basis of stony coral biomineralization: history, trends and future prospects. J. Struct. Biol. 213, 107782 https://doi.org/10.1016/j.jsb.2021.107782.

Dymond, J., Suess, E., Lyle, M., 1992. Barium in Deep-Sea Sediment: a Geochemical Proxy for Paleoproductivity. Paleoceanography 7, 163–181. https://doi.org/10.1029/92PA00181.

Falkner, K.K., Macdonald, R.W., Carmack, E.C., Weingartner, T., 1994. Barium in seawater and sediments from the Artic Ocean. PANGAEA. https://doi.org/10.1594/PANGAEA.734072. Supplement to: Falkner, K. K. et al., 1994. The potential of Barium as a tracer in Arctic water masses. In: Johannessen, O. M., Muench, R. D. & Overland, J. E. (Eds.), The polar oceans and their role in shaping the global environment. Geophysical Monograph Series, American Geophysical Union, 540 pages, ISBN 0-87590-042-9, 85, 63-76.

Gaetani, G.A., Cohen, A.L., 2006. Element partitioning during precipitation of aragonite from seawater: a framework for understanding paleoproxies. Geochim. Cosmochim. Acta 70, 4617–4634. https://doi.org/10.1016/j.gca.2006.07.008.

Gagnon, A.C., Adkins, J.F., Fernandez, D.P., Robinson, L.F., 2007. Sr/Ca and Mg/Ca vital effects correlated with skeletal architecture in a scleractinian deep-sea coral and the role of Rayleigh fractionation. Earth Planet. Sci. Lett. 261, 280–295. https://doi.org/10.1016/j.epsl.2007.07.013.

Ganeshram, R.S., François, R., Commeau, J., Brown-Leger, S.L., 2003. An experimental investigation of barite formation in seawater. Geochim. Cosmochim. Acta 67, 2599–2605. https://doi.org/10.1016/S0016-7037(03)00164-9.

Gattuso, J.-P., Epitalon, J.-M., Lavigne, H., Orr, J., 2021. Seacarb: Seawater Carbonate Chemistry. R Package Version 3.3.0. http://CRAN.R-project.org/package=seacarb.

Geyman, B.M., Ptacek, J.L., LaVigne, M., Horner, T.J., 2019. Barium in deep-sea bamboo corals: phase associations, barium stable isotopes, & prospects for paleoceanography. Earth Planet. Sci. Lett. 525, 115751 https://doi.org/10.1016/j.epsl.2019.115751.

Gillikin, D.P., Dehairs, F., Lorrain, A., Steenmans, D., Baeyens, W., André, L., 2006. Barium uptake into the shells of the common mussel (*Mytilus edulis*) and the potential for estuarine paleo-chemistry reconstruction. Geochim. Cosmochim. Acta 70, 395–407. https://doi.org/10.1016/j.gca.2005.09.015.

Gillikin, D.P., Lorrain, A., Paulet, Y.-M., André, L., Dehairs, F., 2008. Synchronous barium peaks in high-resolution profiles of calcite and aragonite marine bivalve shells. Geo-Mar. Lett. 28, 351–358. https://doi.org/10.1007/s00367-008-0111-9.

Gómez, C.E., Wickes, L., Deegan, D., Etnoyer, P.J., Cordes, E.E., 2018. Growth and feeding of deep-sea coral *Lophelia pertusa* from the California margin under simulated ocean acidification conditions. PeerJ 6, e5671. https://doi.org/10.7717/peerj.5671.

Gonneea, M.E., Cohen, A.L., DeCarlo, T.M., Charette, M.A., 2017. Relationship between water and aragonite barium concentrations in aquaria reared juvenile corals. Geochim. Cosmochim. Acta 209, 123–134. https://doi.org/10.1016/j.gca.2017.04.006.

Griffith, E.M., Paytan, A., 2012. Barite in the ocean - occurrence, geochemistry and palaeoceanographic applications. Sedimentology 59, 1817–1835. https://doi.org/10.1111/j.1365-3091.2012.01327.x.

Hamel, J.-F., Sun, Z., Mercier, A., 2010. Influence of size and seasonal factors on the growth of the deep-sea coral *Flabellum alabastrum* in mesocosm. Coral Reefs 29, 521–525. https://doi.org/10.1007/s00338-010-0590-9.

Hathorne, E.C., Gagnon, A., Felis, T., Adkins, J., Asami, R., Boer, W., Caillon, N., Case, D., Cobb, K.M., Douville, E., deMenocal, P., Eisenhauer, A., Garbe-Schönberg, D., Geibert, W., Goldstein, S., Hughen, K., Inoue, M., Kawahata, H., Kölling, M., Cornec, F.L., Linsley, B.K., McGregor, H.V., Montagna, P., Nurhati, I.S., Quinn, T.M., Raddatz, J., Rebaubier, H., Robinson, L., Sadekov, A., Sherrell, R., Sinclair, D., Tudhope, A.W., Wei, G., Wong, H., Wu, H.C., You, C.-F., 2013. Interlaboratory study for coral Sr/ca and other element/Ca ratio measurements. Geochem. Geophys. Geosyst. 14, 3730–3750. https://doi.org/10.1002/ggge.20230.

Hemsing, F., Hsieh, Y.-T., Bridgestock, L., Spooner, P.T., Robinson, L.F., Frank, N., Henderson, G.M., 2018. Barium isotopes in cold-water corals. Earth Planet. Sci. Lett. 491, 183–192. https://doi.org/10.1016/j.epsl.2018.03.040.

Holcomb, M., Cohen, A.L., Gabitov, R.I., Hutter, J.L., 2009. Compositional and morphological features of aragonite precipitated experimentally from seawater and biogenically by corals. Geochim. Cosmochim. Acta 73, 4166–4179. https://doi.org/10.1016/j.gca.2009.04.015.

Hönisch, B., Allen, K.A., Russell, A.D., Eggins, S.M., Bijma, J., Spero, H.J., Lea, D.W., Yu, J., 2011. Planktic foraminifers as recorders of seawater Ba/ca. Mar. Micropaleontol. 79, 52–57. https://doi.org/10.1016/j.marmicro.2011.01.003.

Hoppema, M., Dehairs, F., Navez, J., Monnin, C., Jeandel, C., Fahrbach, E., de Baar, H.J. W., 2010. Distribution of barium in the Weddell Gyre: Impact of circulation and biogeochemical processes. Mar. Chem. 122, 118–129. https://doi.org/10.1016/j.marchem.2010.07.005.

Horner, T.J., Kinsley, C.W., Nielsen, S.G., 2015. Barium-isotopic fractionation in seawater mediated by barite cycling and oceanic circulation. Earth Planet. Sci. Lett. 430, 511–522. https://doi.org/10.1016/j.epsl.2015.07.027.

Hsieh, Y.-T., Henderson, G.M., 2017. Barium stable isotopes in the global ocean: Tracer of Ba inputs and utilization. Earth Planet. Sci. Lett. 473, 269–278. https://doi.org/10.1016/j.epsl.2017.06.024.

Jeandel, C., Dupré, B., Lebaron, G., Monnin, C., Minster, J.-F., 1996. Longitudinal distributions of dissolved barium, silica and alkalinity in the western and southern Indian Ocean. Deep-Sea Res. I Oceanogr. Res. Pap. 43, 1–31. https://doi.org/10.1016/0967-0637(95)00098-4.

Jurikova, H., Liebetrau, V., Raddatz, J., Fietzke, J., Trotter, J., Rocholl, A., Krause, S., McCulloch, M., Rüggeberg, A., Eisenhauer, A., 2019. Boron isotope composition of the cold-water coral *Lophelia pertusa* along the Norwegian margin: Zooming into a potential pH-proxy by combining bulk and high-resolution approaches. Chem. Geol. 513, 143–152. https://doi.org/10.1016/j.chemgeo.2019.01.005.

Kontoyannis, C.G., Vagenas, N.V., 2000. Calcium carbonate phase analysis using XRD and FT-Raman spectroscopy. Analyst 125, 251–255. https://doi.org/10.1039/a908609i.

Lauvset, S.K., Lange, N., Tanhua, T., Bittig, H.C., Olsen, A., Kozyr, A., Álvarez, M., Becker, S., Brown, P.J., Carter, B.R., Cotrim da Cunha, L., Feely, R.A., van Heuven, S., Hoppema, M., Ishii, M., Jeansson, E., Jutterström, S., Jones, S.D., Karlsen, M.K., Lo Monaco, C., Michaelis, P., Murata, A., Pérez, F.F., Pfeil, B., Schirnick, C., Steinfeldt, R., Suzuki, T., Tilbrook, B., Velo, A., Wanninkhof, R., Woosley, R.J., Key, R.M., 2021. An updated version of the global interior ocean biogeochemical data product, GLODAPv2.2021. Earth Syst. Sci. Data 13, 5565–5589. https://doi.org/10.5194/essd-13-5565-2021.

LaVigne, M., Hill, T.M., Spero, H.J., Guilderson, T.P., 2011. Bamboo coral Ba/ca: Calibration of a new deep ocean refractory nutrient proxy. Earth Planet. Sci. Lett. 312, 506–515. https://doi.org/10.1016/j.epsl.2011.10.013.

LaVigne, M., Grottoli, A.G., Palardy, J.E., Sherrell, R.M., 2016. Multi-colony calibrations of coral Ba/Ca with a contemporaneous in situ seawater barium record. Geochim. Cosmochim. Acta 179, 203–216. https://doi.org/10.1016/j.gca.2015.12.038.

Le Roy, E., Sanial, V., Charette, M.A., van Beek, P., Lacan, F., Jacquet, S.H.M., Henderson, P.B., Souhaut, M., García-Ibáñez, M.I., Jeandel, C., Pérez, F.F., Sarthou, G., 2018. The $^{226}$Ra–Ba relationship in the North Atlantic during GEOTRACES-GA01. Biogeosciences 15, 3027–3048. https://doi.org/10.5194/bg-15-3027-2018.

Lea, D.W., Boyle, E.A., 1991. Barium in planktonic foraminifera. Geochim. Cosmochim. Acta 55, 3321–3331. https://doi.org/10.1016/0016-7037(91)90491-M.

Lea, D.W., Boyle, E.A., 1993. Determination of carbonate-bound barium in foraminifera and corals by isotope dilution plasma-mass spectrometry. Chem. Geol. 103, 73–84. https://doi.org/10.1016/0009-2541(93)90292-Q.

Lea, D.W., Spero, H.J., 1994. Assessing the reliability of paleochemical tracers: Barium uptake in the shells of planktonic foraminifera. Paleoceanograph. Paleoclimatol. 9, 445–452. https://doi.org/10.1029/94PA00151.

Lea, D.W., Shen, G.T., Boyle, E.A., 1989. Coralline barium records temporal variability in equatorial Pacific upwelling. Nature 340, 373–376. https://doi.org/10.1038/340373a0.

Liu, Y., Li, X., Zeng, Z., Yu, H.-M., Huang, F., Felis, T., Shen, C.-C., 2019. Annually-resolved coral skeletal $\delta^{138}/^{134}$Ba records: a new proxy for oceanic Ba cycling. Geochim. Cosmochim. Acta 247, 27–39. https://doi.org/10.1016/j.gca.2018.12.022.

Lueker, T.J., Dickson, A.G., Keeling, C.D., 2000. Ocean $pCO_2$ calculated from dissolved inorganic carbon, alkalinity, and equations for $K_1$ and $K_2$: validation based on laboratory measurements of $CO_2$ in gas and seawater at equilibrium. Mar. Chem. 70, 105–119. https://doi.org/10.1016/S0304-4203(00)00022-0.

Mavromatis, V., Immenhauser, A., Buhl, D., Purgstaller, B., Baldermann, A., Dietzel, M., 2017. Effect of organic ligands on Mg partitioning and Mg isotope fractionation during low-temperature precipitation of calcite in the absence of growth rate effects. Geochim. Cosmochim. Acta 207, 139–153. https://doi.org/10.1016/j.gca.2017.03.020.

Mavromatis, V., Goetschl, K.E., Grengg, C., Konrad, F., Purgstaller, B., Dietzel, M., 2018. Barium partitioning in calcite and aragonite as a function of growth rate. Geochim. Cosmochim. Acta 237, 65–78. https://doi.org/10.1016/j.gca.2018.06.018.

McCorkle, D.C., Martin, P.A., Lea, D.W., Klinkhammer, G.P., 1995. Evidence of a dissolution effect on benthic foraminiferal shell chemistry: $\delta^{13}$C, Cd/Ca, Ba/Ca, and Sr/Ca results from the Ontong Java Plateau. Paleoceanograph. Paleoclimatol. 10, 699–714. https://doi.org/10.1029/95PA01427.

McManus, J., Berelson, W.M., Klinkhammer, G.P., Kilgore, T.E., Hammond, D.E., 1994. Remobilization of barium in continental margin sediments. Geochim. Cosmochim. Acta 58, 4899–4907. https://doi.org/10.1016/0016-7037(94)90220-8.

Mercier, A., Sun, Z., Hamel, J.-F., 2011. Reproductive periodicity, spawning and development of the deep-sea scleractinian coral *Flabellum angulare*. Mar. Biol. 158, 371–380. https://doi.org/10.1007/s00227-010-1565-7.

Montagna, P., McCulloch, M., Douville, E., López Correa, M., Trotter, J., Rodolfo-Metalpa, R., Dissard, D., Ferrier-Pagès, C., Frank, N., Freiwald, A., Goldstein, S., Mazzoli, C., Reynaud, S., Rüggeberg, A., Russo, S., Taviani, M., 2014. Li/Mg systematics in scleractinian corals: Calibration of the thermometer. Geochim. Cosmochim. Acta 132, 288–310. https://doi.org/10.1016/j.gca.2014.02.005.

Mucci, A., Morse, J.W., 1983. The incorporation of $Mg^{2+}$ and $Sr^{2+}$ into calcite overgrowths: influences of growth rate and solution composition. Geochim. Cosmochim. Acta 47, 217–233. https://doi.org/10.1016/0016-7037(83)90135-7.

Nozaki, Y., 1997. A fresh look at element distribution in the North Pacific Ocean. Eos Trans. AGU 78, 221. https://doi.org/10.1029/97EO00148.

Östlund, H.G., Craig, H.C., Broecker, W.S., Spencer, D.W., GEOSECS, 1987. Shorebased measurements during the GEOSECS Pacific expedition. PANGAEA. https://doi.org/10.1594/PANGAEA.743238.

Poulain, C., Gillikin, D.P., Thébault, J., Munaron, J.M., Bohn, M., Robert, R., Paulet, Y.-M., Lorrain, A., 2015. An evaluation of Mg/Ca, Sr/Ca, and Ba/Ca ratios as environmental proxies in aragonite bivalve shells. Chem. Geol. 396, 42–50. https://doi.org/10.1016/j.chemgeo.2014.12.019.

Pretet, C., Zuilen, K., Nägler, T.F., Reynaud, S., Böttcher, M.E., Samankassou, E., 2015. Constraints on barium isotope fractionation during aragonite precipitation by corals. Deposition. Rec. 1, 118–129. https://doi.org/10.1002/dep2.8.

Pyle, K.M., Hendry, K.R., Sherrell, R.M., Legge, O., Hind, A.J., Bakker, D., Venables, H., Meredith, M.P., 2018. Oceanic fronts control the distribution of dissolved barium in

the Southern Ocean. Mar. Chem. 204, 95–106. https://doi.org/10.1016/j.marchem.2018.07.002.

Raddatz, J., Liebetrau, V., Rüggeberg, A., Hathorne, E., Krabbenhöft, A., Eisenhauer, A., Böhm, F., Vollstaedt, H., Fietzke, J., López Correa, M., Freiwald, A., Dullo, W.-Chr., 2013. Stable Sr-isotope, Sr/Ca, Mg/Ca, Li/Ca and Mg/Li ratios in the scleractinian cold-water coral *Lophelia pertusa*. Chem. Geol. 352, 143–152. https://doi.org/10.1016/j.chemgeo.2013.06.013.

Rae, J.W.B., Foster, G.L., Schmidt, D.N., Elliott, T., 2011. Boron isotopes and B/Ca in benthic foraminifera: Proxies for the deep ocean carbonate system. Earth Planet. Sci. Lett. 302, 403–413. https://doi.org/10.1016/j.epsl.2010.12.034.

Reed, E.V., Thompson, D.M., Cole, J.E., Lough, J.M., Cantin, N.E., Cheung, A.H., Tudhope, A., Vetter, L., Jimenez, G., Edwards, R.L., 2021. Impacts of Coral Growth on Geochemistry: Lessons from the Galápagos Islands. Paleoceanograph. Paleoclimatol. 36 https://doi.org/10.1029/2020PA004051.

Roeske, T., Rutgers van der Loeff, M.M., 2012. Barium measured on water bottle samples during POLARSTERN cruise ANT-XXIV/3. PANGAEA. https://doi.org/10.1594/PANGAEA.786619.

Ross, C.L., DeCarlo, T.M., McCulloch, M.T., 2019. Calibration of Sr/Ca, Li/Mg and Sr-U Paleothermometry in Branching and Foliose Corals. Paleoceanograph. Paleoclimatol. 34, 1271–1291. https://doi.org/10.1029/2018PA003426.

Samperiz, A., Robinson, L.F., Stewart, J.A., Strawson, I., Leng, M.J., Rosenheim, B.E., Ciscato, E.R., Hendry, K.R., Santodomingo, N., 2020. Stylasterid corals: a new paleotemperature archive. Earth Planet. Sci. Lett. 545, 116407 https://doi.org/10.1016/j.epsl.2020.116407.

Sathyendranath, S., Brewin, R., Brockmann, C., Brotas, V., Calton, B., Chuprin, A., Cipollini, P., Couto, A., Dingle, J., Doerffer, R., Donlon, C., Dowell, M., Farman, A., Grant, M., Groom, S., Horseman, A., Jackson, T., Krasemann, H., Lavender, S., Martinez-Vicente, V., Mazeran, C., Mélin, F., Moore, T., Müller, D., Regner, P., Roy, S., Steele, C., Steinmetz, F., Swinton, J., Taberner, M., Thompson, A., Valente, A., Zühlke, M., Brando, V., Feng, H., Feldman, G., Franz, B., Frouin, R., Gould, R., Hooker, S., Kahru, M., Kratzer, S., Mitchell, B., Muller-Karger, F., Sosik, H., Voss, K., Werdell, J., Platt, T., 2019. An Ocean-Colour Time Series for use in climate Studies: the experience of the Ocean-Colour climate Change Initiative (OC-CCI). Sensors 19, 4285. https://doi.org/10.3390/s19194285.

Sathyendranath, S., Jackson, T., Brockmann, C., Brotas, V., Calton, B., Chuprin, A., Clements, O., Cipollini, P., Danne, O., Dingle, J., Donlon, C., Grant, M., Groom, S., Krasemann, H., Lavender, S., Mazeran, C., Mélin, F., Müller, D., Steinmetz, F., Valente, A., Zühlke, M., Feldman, G., Franz, B., Frouin, R., Werdell, J., Platt, T., 2021. ESA Ocean Colour Climate Change Initiative (Ocean_Colour_cci): Version 5.0 Data. https://doi.org/10.5285/1DBE7A109C0244AAAD713E078FD3059A.

Schlitzer, R., 2022. Ocean Data View. https://odv.awi.de.

Serrato Marks, G., LaVigne, M., Hill, T.M., Sauthoff, W., Guilderson, T.P., Roark, E.B., Dunbar, R.B., Horner, T.J., 2017. Reproducibility of Ba/Ca variations recorded by Northeast Pacific bamboo corals. Paleoceanograph. Paleoclimatol. 32, 966–979. https://doi.org/10.1002/2017PA003178.

Sinclair, D.J., Risk, M.J., 2006. A numerical model of trace-element coprecipitation in a physicochemical calcification system: Application to coral biomineralization and trace-element 'vital effects.'. Geochim. Cosmochim. Acta 70, 3855–3868. https://doi.org/10.1016/j.gca.2006.05.019.

Smetacek, V., de Baar, H.J.W., Bathmann, U., Lochte, K., Rutgers van der Loeff, M.M., 1997. Biogeochemistry of barium measured on water bottle samples during POLARSTERN cruise ANT-X/6. PANGAEA. https://doi.org/10.1594/PANGAEA.88250. Supplement to: Smetacek, V. et al., 1997. Ecology and biogeochemistry of the Antarctic circumpolar current during austral spring: Southern Ocean JGOFS Cruise ANT X/6 of R.V. Polarstern. *Deep Sea Research Part II: Topical Studies in Oceanography*, 44(1-2), 1-21, https://doi.org/10.1016/S0967-0645(96)00100-2.

Spooner, P.T., Robinson, L.F., Hemsing, F., Morris, P., Stewart, J.A., 2018. Extended calibration of cold-water coral Ba/ca using multiple genera and co-located measurements of dissolved barium concentration. Chem. Geol. 499, 100–110. https://doi.org/10.1016/j.chemgeo.2018.09.012.

Sternberg, E., Tang, D., Ho, T.-Y., Jeandel, C., Morel, F.M.M., 2005. Barium uptake and adsorption in diatoms. Geochim. Cosmochim. Acta 69, 2745–2752. https://doi.org/10.1016/j.gca.2004.11.026.

Stewart, J.A., Robinson, L.F., Day, R.D., Strawson, I., Burke, A., Rae, J.W.B., Spooner, P.T., Samperiz, A., Etnoyer, P.J., Williams, B., Paytan, A., Leng, M.J., Häussermann, V., Wickes, L.N., Bratt, R., Pryer, H., 2020a. Refining trace metal temperature proxies in cold-water scleractinian and stylasterid corals. Earth Planet. Sci. Lett. 545, 116412 https://doi.org/10.1016/j.epsl.2020.116412.

Stewart, J.A., Christopher, S.J., Kucklick, J.R., Bordier, L., Chalk, T.B., Dapoigny, A., Douville, E., Foster, G.L., Gray, W.R., Greenop, R., Gutjahr, M., Hemsing, F., Henehan, M.J., Holdship, P., Hsieh, Y., Kolevica, A., Lin, Y., Mawbey, E.M., Rae, J.W.B., Robinson, L.F., Shuttleworth, R., You, C., Zhang, S., Day, R.D., 2020b. NIST RM 8301 Boron Isotopes in Marine Carbonate (simulated Coral and Foraminifera Solutions): Inter-laboratory $\delta^{11}B$ and Trace Element Ratio Value Assignment. Geostand. Geoanal. Res. 45, 77–96. https://doi.org/10.1111/ggr.12363.

Stewart, J.A., Strawson, I., Kershaw, J., Robinson, L.F., 2022. Stylasterid corals build aragonite skeletons in undersaturated water despite low pH at the site of calcification. Sci. Rep. 12, 13105. https://doi.org/10.1038/s41598-022-16787-y.

Stolarski, J., Coronado, I., Murphy, J.G., Kitahara, M.V., Janiszewska, K., Mazur, M., Gothmann, A.M., Bouvier, A.-S., Marin-Carbonne, J., Taylor, M.L., Quattrini, A.M., McFadden, C.S., Higgins, J.A., Robinson, L.F., Meibom, A., 2021. A modern scleractinian coral with a two-component calcite–aragonite skeleton. Proc. Natl. Acad. Sci. U. S. A. 118, e2013316117 https://doi.org/10.1073/pnas.2013316117.

Tang, D., Morel, F.M.M., 2006. Distinguishing between cellular and Fe-oxide-associated trace elements in phytoplankton. Mar. Chem. 98, 18–30. https://doi.org/10.1016/j.marchem.2005.06.003.

Therneau, T., 2018. Deming: Deming, Theil-Sen, Passing-Bablock and Total Least Squares Regression. R Package Version 1.4. https://CRAN.R-project.org/package=deming.

Thresher, R.E., Fallon, S.J., Townsend, A.T., 2016. A "core-top" screen for trace element proxies of environmental conditions and growth rates in the calcite skeletons of bamboo corals (Isididae). Geochim. Cosmochim. Acta 193, 75–99. https://doi.org/10.1016/j.gca.2016.07.033.

Ulrich, R.N., Guillermic, M., Campbell, J., Hakim, A., Han, R., Singh, S., Stewart, J.D., Román-Palacios, C., Carroll, H.M., De Corte, I., Gilmore, R.E., Doss, W., Tripati, A., Ries, J.B., Eagle, R.A., 2021. Patterns of Element Incorporation in Calcium Carbonate Biominerals Recapitulate Phylogeny for a Diverse Range of Marine Calcifiers. Front. Earth Sci. 9, 641760 https://doi.org/10.3389/feart.2021.641760.

Watson, E.B., 2004. A conceptual model for near-surface kinetic controls on the trace-element and stable isotope composition of abiogenic calcite crystals. Geochim. Cosmochim. Acta 68, 1473–1488. https://doi.org/10.1016/j.gca.2003.10.003.